applied sciences

MDPI

Article

Test and Numerical Study on Blast Resistance of Main Girders Coated with Polyurea in Self-Anchored Suspension Bridges

Rong Wang, Guangpan Zhou * and Xiaobao Zuo

School of Science, Nanjing University of Science and Technology, Nanjing 210094, China; 121113223332@njust.edu.cn (R.W.); xbzuo@njust.edu.cn (X.Z.)
* Correspondence: guangpanzhou@njust.edu.cn

Abstract: This study investigates the blast-resistant performance of a polyurea-coated suspension bridge girder under explosive loads. The Hunan Road Bridge of Shandong was used as a case study through combined test and numerical simulation methods. Two 3 kg TNT charges and one 5 kg TNT charge were used to conduct two single-blast tests and one repeated blast test on a 1:3 scaled segment of a box girder. The tests were labeled as G (box girder without polyurea), PCG (first blast on box girder coated with polyurea), and PCGR (second blast on box girder coated with polyurea). A 1.5 mm polyurea layer was uniformly applied to the top surface. Numerical simulations of the explosion response were performed and validated using LS-DYNA software. The results indicate that under 3 kg of TNT detonation directly above the top plate, sample G exhibited an elliptical perforation, whereas sample PCG only experienced minor local dents without penetration. After a second detonation of 5 kg of TNT above the box chambers, sample PCGR displayed a nearly circular perforation in the top plate, along with cracks near the supports of chambers 1 and 3. For the main girder of the suspension bridge, multiple detonation points caused severe damage, rendering it impassable. However, after polyurea coating, the blast resistance significantly improved, with only minor spalling of concrete on the top plate and no other notable damage, allowing for continued passage. The polyurea layer effectively reduced the vertical displacement of the girder, and this reduction plateaued with increasing coating thickness. Under a 500 kg TNT blast, the optimal polyurea thickness to enhance blast resistance was determined to be 9 mm.

Keywords: self-anchored suspension bridge; concrete box girder; explosion-resisting performance; protection with polyurea; repeated explosion; numerical simulation

Citation: Wang, R.; Zhou, G.; Zuo, X. Test and Numerical Study on Blast Resistance of Main Girders Coated with Polyurea in Self-Anchored Suspension Bridges. *Appl. Sci.* **2024**, *14*, 9280. https://doi.org/10.3390/app14209280

Academic Editor: Syed Minhaj Saleem Kazmi

Received: 20 September 2024
Revised: 9 October 2024
Accepted: 10 October 2024
Published: 12 October 2024

1. Introduction

With the continued growth of the global economy, transportation systems have developed significantly. As a core component of transportation networks, bridges play a critical role in national infrastructure, as well as in military and economic sectors [1,2]. Even under exceptional circumstances, it is essential to monitor the protective status of existing reinforced concrete bridges [3,4]. In recent years, with the intensification of international conflicts, bridges, being critical nodes in transportation networks, have become prime targets for terrorist attacks and localized warfare. Over the past three decades, global terrorist activities have shown a notable upward trend, with the "911" attacks standing out as the most well-known example. This event not only caused significant casualties and property damage but also had profound implications for global political, economic, and security landscapes. Due to their openness and relatively low level of security, bridges are often targeted in terrorist attacks. According to reports, between 2002 and 2008, 187 terrorist attacks on bridges occurred worldwide, with car bombs being the primary method of attack. The power and location of the explosion can result in varying degrees of damage to the bridge. The blast shockwaves can damage critical structural components of the bridge, potentially leading to functional failure or, in severe cases, the total collapse of the

bridge, posing a serious threat to human life and socioeconomic development. Several incidents of terrorist attacks and accidents involving vehicles transporting flammable and explosive materials have resulted in severe disasters for bridge structures globally. For example, in 2007, the Sarafiyah Bridge in Baghdad, Iraq, was subjected to a car bomb attack, leading to its progressive collapse and resulting in the death of 10 people. In 2009, two trucks carrying butter and fireworks collided on the Fengxingpai Bridge of the Daguang Expressway in Jiangxi Province, China. The ensuing fire and explosion caused one hollow slab to break and fall, severely damaging seven others and leading to extensive destruction of the bridge. In 2023, the Sitong River Bridge in Myanmar suffered a bomb attack, destroying approximately 65 feet of the bridge deck and severing two piers. Additionally, because of the strategic importance of bridges for troop movement and material transport, military actions targeting bridges are also frequent. For instance, in 1945, the Ludendorff Bridge collapsed following sustained shelling and previous structural damage from unexploded ordnance. In 1993, during the Bosnian War, the Mostar Old Bridge was shelled by the Croatian Defence Council (HVO), eventually collapsing after enduring continuous bombardment. In 2022, during the Russian invasion of Ukraine, an explosion occurred on the Crimean Bridge, which connects the Crimean Peninsula with Russia's Krasnodar Krai, igniting seven fuel tanker cars on the railway section of the bridge and causing three fatalities, as well as partial roadway collapse. In 2023, following the October 2022 explosion of a truck on the Crimean Bridge that caused a railway tanker fire and disrupted road traffic, the Crimean Bridge was again attacked by two unmanned surface vessels, resulting in the road bridge being disabled and the death of two individuals. These attacks not only caused significant damage to the bridges themselves but also led to transportation disruptions and impeded material supplies, dealing major strategic blows to adversaries. From these examples, it is evident that transportation bridges, due to their importance in logistics and strategic mobility, have become key targets in warfare. Striking these targets can weaken the enemy's strategic capabilities and logistical support, thereby exerting a significant influence on the course of the conflict.

Polyurea elastomer is a polymeric compound formed through a rapid cross-linking polymerization reaction between isocyanate components and amine compounds. Due to its unique molecular structure, the chemical reaction of polyurea elastomer is essentially the interaction between semi-prepolymers, amino polyether, and amine chain extenders. By adjusting the chain extenders and other reactants, the mechanical properties of polyurea elastomers can be enhanced. Moreover, the cleavage of hydrogen bonds within the hard segments of the microstructure allows for partial energy absorption, which contributes to its excellent mechanical properties and energy-dissipation mechanism. These characteristics provide a solid foundation for the study of polyurea elastomer's response to explosive impact. Polyurea elastomers have garnered significant attention from numerous experts and scholars for their exceptional performance in enhancing the blast and penetration resistance of structures [5–10]. In 1996, the Air Force Research Laboratory (AFRL) first selected polyurea from 21 elastomeric materials as an impact-resistant protective coating [11,12]. Regarding masonry structures, Pu [13] conducted a simulation analysis on polyurea-coated masonry walls. By comparing the damage to the central section of walls with and without polyurea coating under a 50 kg TNT explosion, it was found that uncoated masonry experienced severe damage with substantial fragmentation, while the polyurea-coated masonry showed significantly less damage with almost no debris ejection, indicating that polyurea can enhance the blast resistance of masonry structures. Baylot et al. [14] explored the blast resistance of masonry walls reinforced with various methods, including fiber-reinforced composites, galvanized steel sheets, and polyurea elastomer coatings. The results of their blast tests demonstrated that walls reinforced with polyurea coatings maintained better structural integrity and effectively contained debris within the structure. For steel structures, Ackland [7] investigated the impact of polyurea coatings on the failure of steel plates under explosive loads. Their experimental results revealed that steel plates with polyurea coatings exhibited greater residual deformation, with the

degree of deformation increasing as the coating thickness increased. Samiee [15] conducted a simulation analysis on the dynamic response and deformation of circular steel plates with and without polyurea coatings. Their findings showed that polyurea-coated steel plates exhibited superior blast resistance compared to uncoated plates. Notably, plates coated with polyurea on the back side of the blast showed better blast resistance than those coated on the front side or without any coating. Additionally, the difference in blast resistance became more pronounced with increasing polyurea coating thickness.

A substantial body of research has been conducted by both domestic and international scholars on the blast damage behavior of bridge structures. In the field of concrete box girders, Wang [16] employed ANSYS/LS-DYNA software (https://www.lstc.com/products/ls-dyna) to analyze the damage response of a three-tower, double-cable, self-anchored suspension bridge subjected to varying explosive charges and detonation heights. The study identified the minimum charge necessary to cause damage under different conditions. Yang [17] examined the failure behaviors of reinforced concrete box girders through both blast experiments and numerical simulations. Qiu [18] utilized ANSYS/LS-DYNA software to investigate the dynamic behavior and failure modes of prestressed concrete box girders under different TNT charge amounts, blast positions, and levels of prestress loss. Fujikura et al. [19], William et al. [20], Echevarria [21], Williamson [22], and Islam [23] conducted multiple experimental investigations focused on the blast effects on bridge pier components. In the domain of concrete T-beams, Maazoun [24] conducted full-scale blast tests on prestressed T-beams and identified localized shear failure of the concrete as the primary failure mode. Han [25] conducted model tests on prestressed T-beams simulating terrorist explosions on bridge decks, noting that with increasing explosive charge, the damage to prestressed steel tendons intensified, the frequency of anchorage failures increased, and the steel tendons ultimately fractured. As for steel box girders, Yao [26] analyzed the damage modes of various components of steel box girders when car bombs were detonated inside them, suggesting that measures such as the proper arrangement of stiffeners, rebar of critical components, and installation of blast-resistant layers are effective in enhancing the blast resistance of bridges. Hashemi [27] analyzed the dynamic behavior of a cable-stayed steel box girder bridge under different TNT charges and blast locations, highlighting that the detonation height significantly influences the damage modes and plastic deformation of the main girder. In terms of deck systems, Hajek [28] performed large-scale explosion tests to determine the resistance of composite concrete bridge decks when subjected to explosive charges at close range.

Currently, the research on the blast damage effects of bridge girders primarily focuses on steel box girders and concrete T-beams, with relatively limited studies addressing the blast damage behavior of multi-chamber concrete box girders. Furthermore, most of these studies rely on numerical simulations, with a lack of corresponding experimental investigations. In light of the proven effectiveness of polyurea blast protection in masonry and steel structures, there is a pressing need for research on its application in the field of bridge engineering. However, the effectiveness of applying polyurea protective coatings to enhance the blast resistance of concrete box girders in self-anchored suspension bridges remains unclear at present.

In this study, three blast tests were conducted on two identical scaled-down (1:3) specimens of a typical single-box, triple-chamber concrete box girder, based on an actual bridge engineering background. The tests involved two 3 kg of TNT charges and one 5 kg TNT charge. The specimens were designated as G (box girder without polyurea), PCG (box girder coated with polyurea, first detonation), and PCGR (box girder coated with polyurea, second detonation). A comparative analysis was performed to examine the damage characteristics and dynamic response of specimens G, PCG, and PCGR. Simulations were performed utilizing the LS-DYNA software to investigate the damage behavior of concrete box girders coated with polyurea under near-field blast loads. The blast response of polyurea-coated wide box girders was analyzed considering variations in standoff distance, charge position, and detonation method. The findings provide insights that could

serve as a reference for the blast-resistant design of bridges. The technical flowchart of this study is shown in Figure 1.

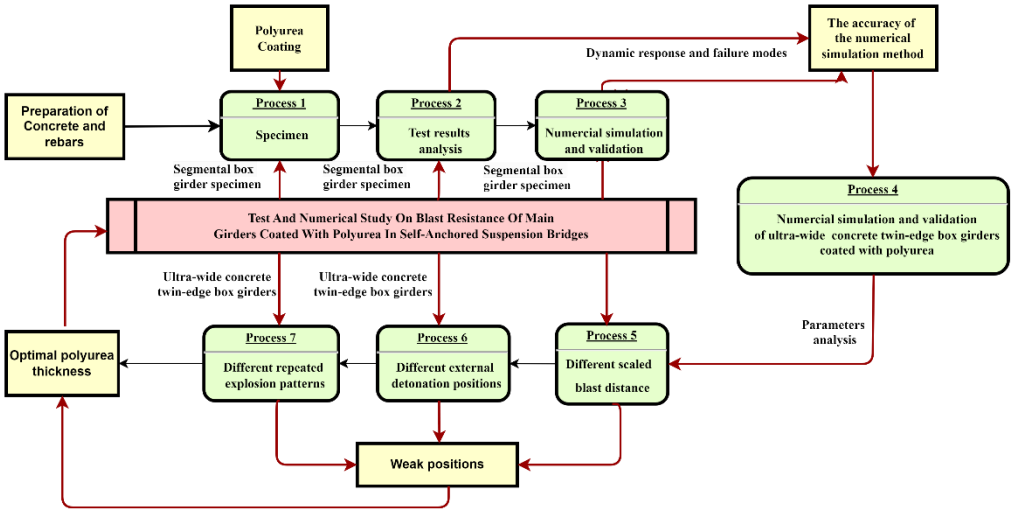

Figure 1. Technique flowchart.

2. Test and Result Analysis

2.1. Specimen

In this study, two 1:3 scale segment specimens were fabricated based on the Shandong Hunan Road Bridge [29], with dimensions provided in Figure 2. The experimental model consists of two parts: a reinforced concrete box girder and six 400 mm × 400 mm brick masonry support columns. Four of the masonry supports beneath the box segment are 600 mm in height, while two supports beneath the long cantilever end are 1453 mm in height. Cement mortar was used to adhere and secure the box girder and masonry supports. Since the primary objective of this test is to assess the dynamic response and failure characteristics of the box girder segment under blast loading [30], the constraints applied to the specimen do not fully replicate real bridge conditions, but they are adequate for model validation.

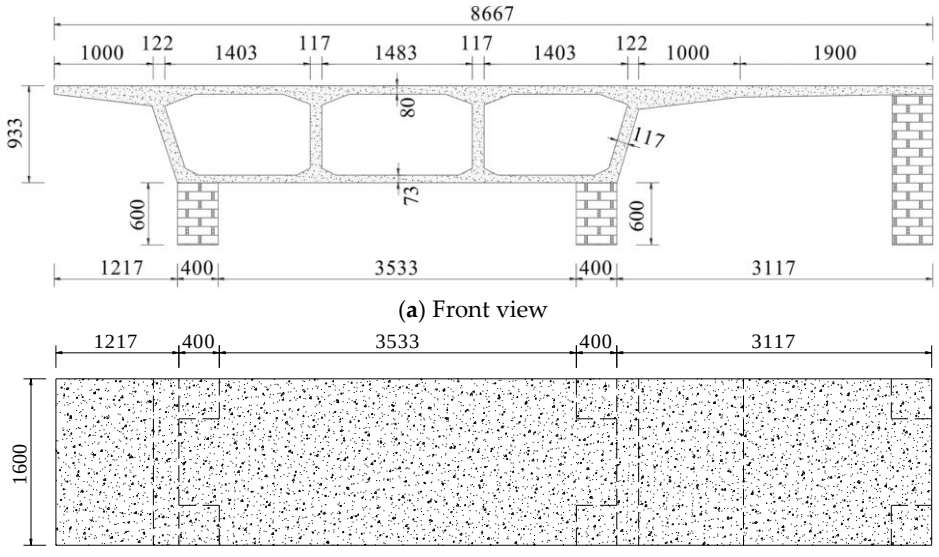

(**a**) Front view

(**b**) Top view

Figure 2. Layout of girder specimen (unit: mm).

The polyurea elastomer used in this study was sourced from Shaanxi Juao Building Materials Co., Ltd. (Xi'an, China) [31]. First, the top surface of the PCG box girder specimen

was cleaned, and the polyurea mixture was applied to the top plate of the PCG specimen with a thickness controlled at 1.5 mm [32]. The real-world conditions of the segmental box girder specimens G and PCG are depicted in Figure 3. Specimen PCGR was used for the second detonation test following the initial detonation of the PCG specimen. The concrete used for the box girder had a grade of C30, and the rebar consisted of 8 mm-diameter ribbed HRB400 steel bars arranged in a double-layer, bidirectional layout with a spacing of 100 mm. The concrete cover thickness was 20 mm. Three standard cubic test blocks were cast from the same batch and cured under the same conditions as the box girder specimens for 28 days. A universal servo-hydraulic machine was used in the laboratory to perform compression tests on the cubes, yielding compressive strengths of 30.5 MPa, 30.8 MPa, and 30.7 MPa, with an average value of 30.7 MPa [30].

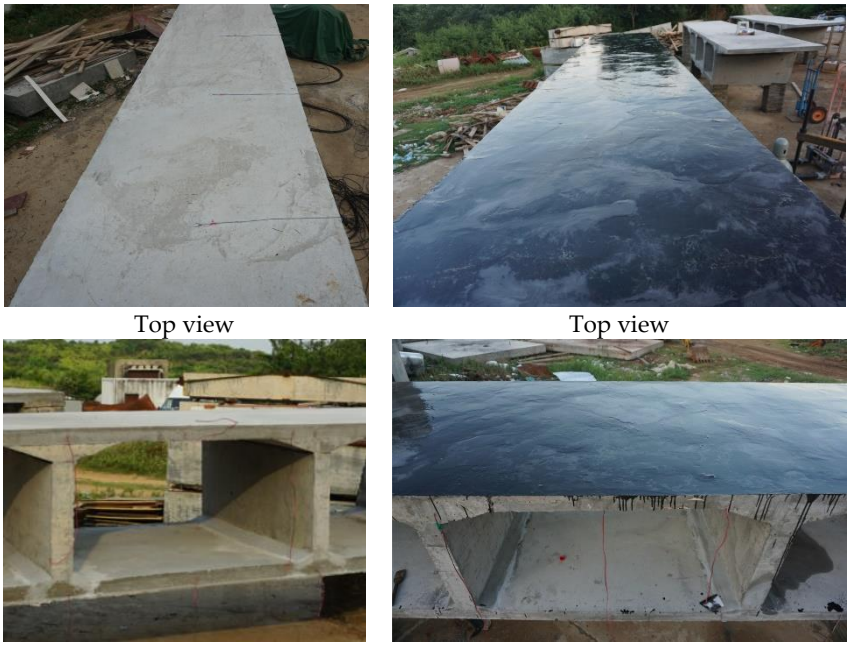

(**a**) G (**b**) PCG

Figure 3. Scene of the segmental girder specimen.

2.2. Layouts of TNT Charge and Measuring Point

Three TNT charges from the same manufacturer and batch were employed, with individual charge masses of 3 kg, 3 kg, and 5 kg, respectively. The blast charge was positioned 0.40 m above the center of the top plate in chamber 2. The detonation was initiated by setting a booster on top of the TNT charge, which was ignited using an electric detonator. Table 1 provides the experimental conditions, and the overall setup of the blast experiment of the specimen is illustrated in Figure 4.

Table 1. Explosion test scenario.

Specimen	Protective Coating	Blast Position	Blast Height/m	TNT Equivalent/kg
G	Without polyurea	The center of the top plate in chamber 2	0.4	3
PCG	With polyurea			3
PCGR	With polyurea			5

The key parameters measured during the blast tests on the box girder include overpressure from shock waves, strain on the reinforcement bars, vertical deflection, and acceleration. Figure 5 illustrates the layout of the strain gauges positioned on the rebar. The placement of measurement points for overpressure, displacement, and acceleration is shown in Figure 6.

Figure 4. In situ arrangement of the explosion test.

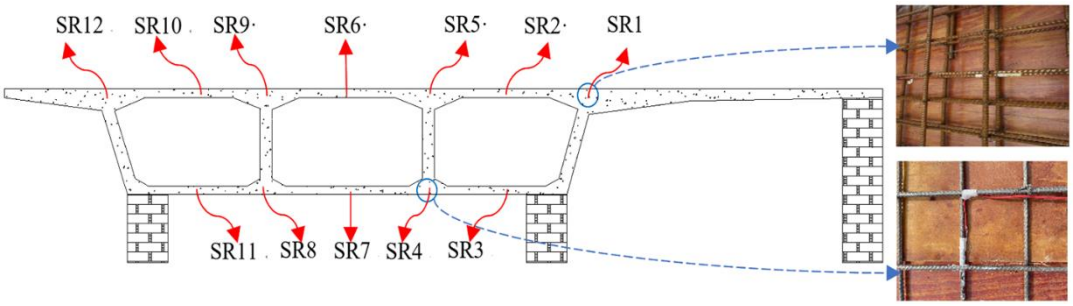

Figure 5. Measuring point of rebar strain.

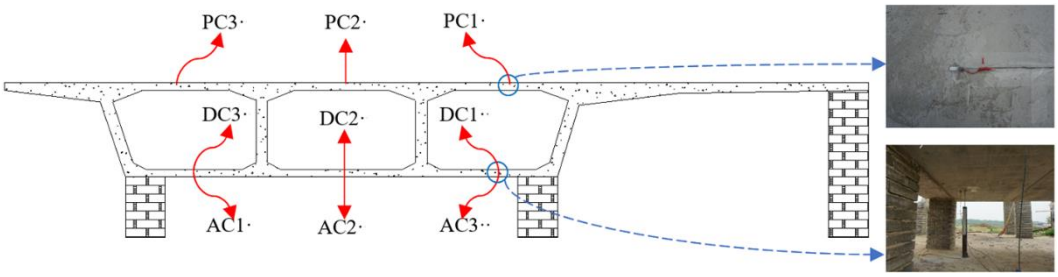

Figure 6. Placement of measurement for overpressure, displacement, and acceleration.

2.3. Test Results Analysis

2.3.1. Shock Wave Overpressure

The blast wave overpressure can be determined using the CONWEP formula. The equation for this calculation is as follows [30]:

$$p = \begin{cases} p_r \cos^2\theta + p_i(1 + \cos^2\theta - 2\cos\theta) & \cos\theta > 0 \\ p_i & \cos\theta \leq 0 \end{cases} \quad (1)$$

where p denotes the blast load pressure, p_r refers to the reflected overpressure, and p_i signifies the incident overpressure. Additionally, the angle of incidence is represented by θ.

As shown in Figure 7, taking the effective measurement point PC1 at the top plate of box chamber 1 of specimens G, PCG, and PCGR as an example, the experimentally measured shock wave overpressure values were compared with those calculated using the CONWEP empirical formula. The error rates were 6.5%, 7.32%, and 6.30%, respectively. The peak overpressure values and the variation trends at the same measurement points

for specimens G, PCG, and PCGR showed good agreement, confirming the validity of the applied blast loading in the experiment.

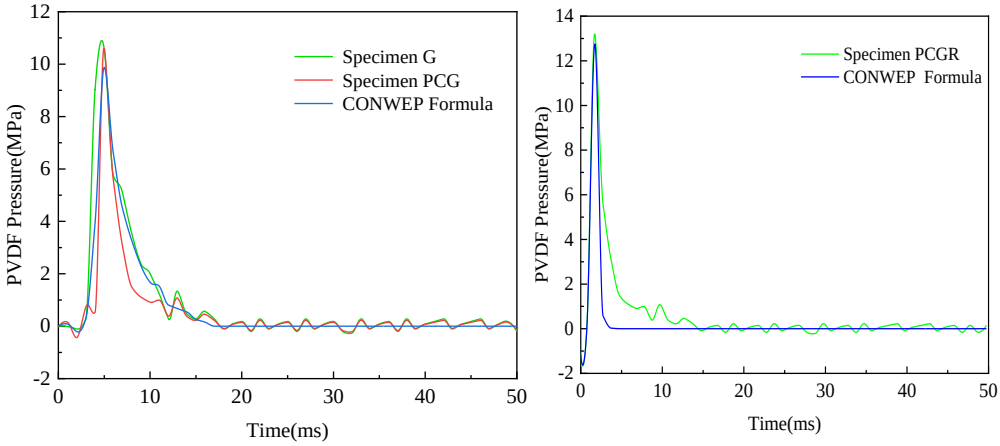

(**a**) Specimen G and PCG (**b**) Specimen G and PCG

Figure 7. Comparison of overpressure of explosion shock wave.

2.3.2. Damage Characteristics

As depicted in Figure 8, under a single detonation of 3 kg of TNT, an elliptical perforation appeared on the top plate of chamber 2 of G, with a size of 41.50 cm (longitudinal direction) × 45.50 cm (transverse direction). In addition, a large area of concrete spalling occurred on the bottom surface, with exposed steel bars and no obvious damage in other areas. As depicted in Figure 9, PCG only showed a slight local indentation with a size of 20 cm × 30.50 cm, and only a small amount of bubbles and signs of carbonization appeared on the surface of the polyurea, with no other damage detected. The polyurea coating remains intact and effectively wraps around the box girder. Comparing the damage of sample G and PCG, it can be seen that the polyurea is capable of absorbing a portion of the explosion energy, resulting in superior blast resistance for PCG compared to G. The damage characteristics of PCGR under secondary detonation are depicted in Figure 10. After the second blast with a charge of 5 kg, a nearly circular perforation measuring 52.90 cm × 58.90 cm was observed on the top plate of the mid-chamber. In addition, obvious cracks were found near the supports of compartments 1 and 3, although no obvious peeling or damage was found on the top and baseplates of other compartments. The comparison of damage characteristics between specimens PCG and PCGR shows that for polyurea-coated reinforced concrete beams with box sections exposed to repeated explosions, the material near the explosion center deteriorates after the initial explosion, leading to the formation of defects. These defects led to a rapid increase in damage during the subsequent explosion, greatly reducing the structural resistance of the box section to the explosion effect.

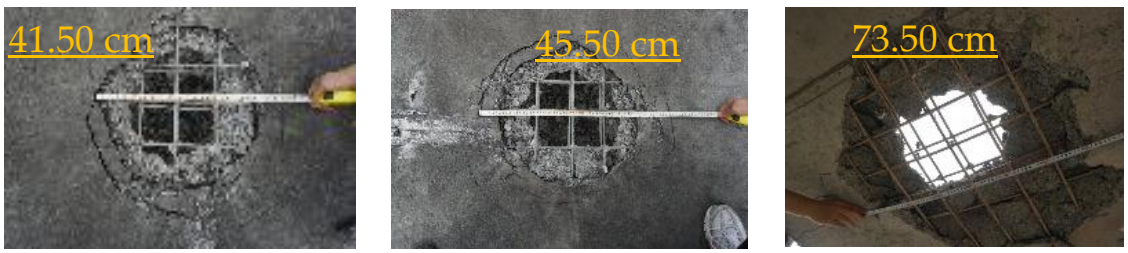

Figure 8. Dimensions of the hole of mid-chamber (G). (**a**) Dimensions of the hole of the top surface (longitudinal direction). (**b**) Dimensions of the hole of the top surface (transverse direction). (**c**) Dimensions of the hole of the bottom surface (transverse direction).

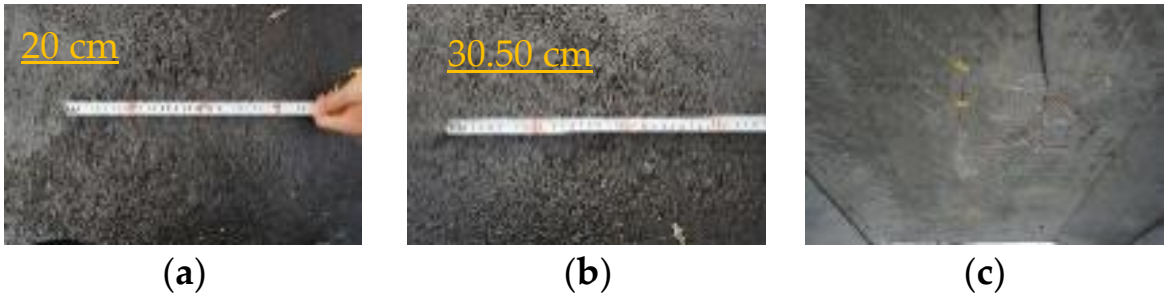

Figure 9. Dimensions of the hole of mid-chamber (PCG). (**a**) Dimensions of the hole of the top surface (longitudinal direction). (**b**) Dimensions of the hole of the top surface (transverse direction). (**c**) No damage.

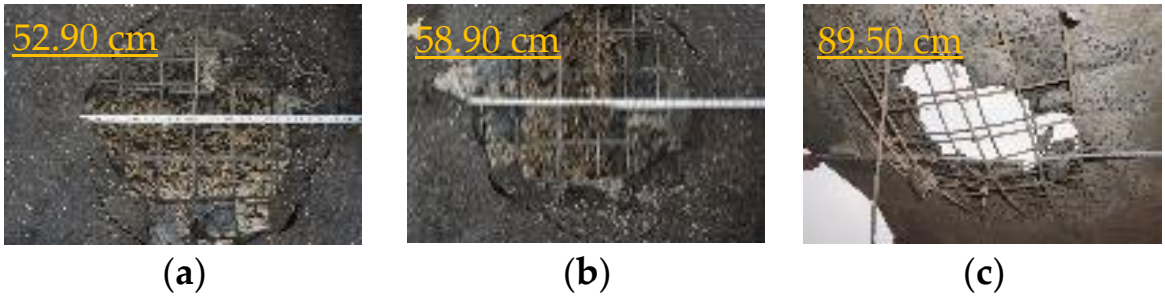

Figure 10. Dimensions of the hole of mid-chamber (PPCG). (**a**) Dimensions of the hole of the top surface (longitudinal direction). (**b**) Dimensions of the hole of the top surface (transverse direction). (**c**) Dimensions of the hole of the bottom surface (transverse direction).

2.3.3. Vertical Displacement

Figure 11 shows the dynamic vertical displacement curves at the center of each compartment's baseplate for specimens G, PCG, and PCGR. Under explosive loading, all specimens exhibited a rapid increase in displacement, followed by a rebound and oscillation process, eventually stabilizing with residual deformation. For specimen G, the maximum vertical displacements at the centers of chambers 1, 2, and 3 were 8.68 mm, 19.26 mm, and 4.87 mm, respectively, with corresponding residual displacements of 2.58 mm, 4.68 mm, and 1.60 mm. This indicates that the explosive impact varied significantly across different locations, with chamber 2, located closest to the blast center, experiencing the most pronounced deformation. In the case of specimen PCG, subjected to the same explosive load, its displacement response was significantly reduced. The maximum vertical displacements in chambers 1, 2, and 3 were 2.93 mm, 4.86 mm, and 2.13 mm, with residual displacements of 0.84 mm, 1.23 mm, and 0.64 mm, respectively. Notably, the peak and residual displacements of compartment 2, directly beneath the blast center, were reduced by 74.8% and 73.7%, respectively, compared to specimen G. This clearly demonstrates the effectiveness of the polyurea coating in mitigating structural deformation induced by the explosion. For specimen PCGR, subjected to repeated explosive loads, the displacement response increased markedly. The maximum vertical displacements in compartments 1, 2, and 3 were 15.61 mm, 34.39 mm, and 8.09 mm, with residual displacements of 2.89 mm, 8.85 mm, and 2.90 mm, respectively. This highlights the significant cumulative damage effect on the box girder under repeated explosive loads, further amplifying the displacement response. In conclusion, the comparative analysis of the displacement patterns of specimens G, PCG, and PCGR reveals that while the polyurea coating effectively reduces displacement under a single explosive load, the cumulative damage effect under repeated explosive loads is substantial, leading to increased displacement response.

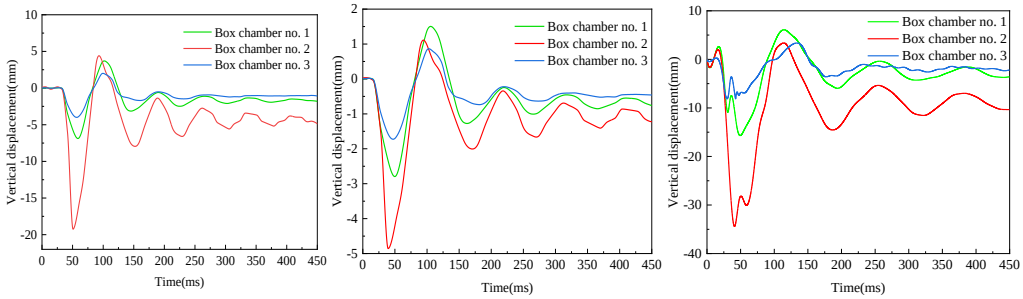

(**a**) Specimen G (**b**) Specimen PCG (**c**) Specimen PCGR

Figure 11. Test results of vertical shift of the baseplate.

2.3.4. Rebar Strain

Figure 12 shows the temporal evolution curves of the rebar strain at the effective measurement points of specimen G. After the blast, the rebar strain rapidly increased to a peak value, then it underwent oscillations and gradually decayed. As the measurement points approached the blast center, the peak strain significantly increased, with residual strain observed at points SR5 and SR7, which are closest to the blast center. Figure 13 shows the rebar strain time-history curves for specimen PCG. Similarly, significant residual strain was observed at measurement points SR6 and SR7, located near the blast center. A comparative analysis of the rebar strain at corresponding measurement points in specimens G and PCG reveals a high degree of similarity in both tensile and compressive strain peaks [30]. Figure 14 shows the time–history curves of rebar strain for specimen PCGR. When comparing the corresponding measurement points in PCG and PCGR, it was observed that the peak strain during the second explosion in PCGR was markedly higher than that of the first explosion. This increase is primarily attributed to the damage and defects formed within the box girder after the first explosion, which weakened the structure's blast resistance. Additionally, residual strain was also observed at measurement points SR1 and SR2, farther from the blast center. In summary, by comparing the time–history curves of rebar strain at different measurement points across specimens G, PCG, and PCGR, the conclusions are as follows: the peak rebar strain in the specimens is significantly influenced by the proximity to the blast center—the closer to the explosion, the higher the peak strain. Furthermore, the increased peak strain observed in specimen PCGR during the second explosion indicates the cumulative damage effect on the structure under repeated explosive loads.

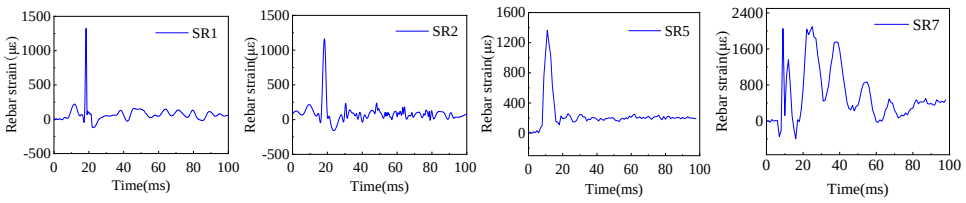

(**a**) SR1 (**b**) SR2 (**c**) SR5 (**d**) SR7

Figure 12. Measured rebar strain of specimen G.

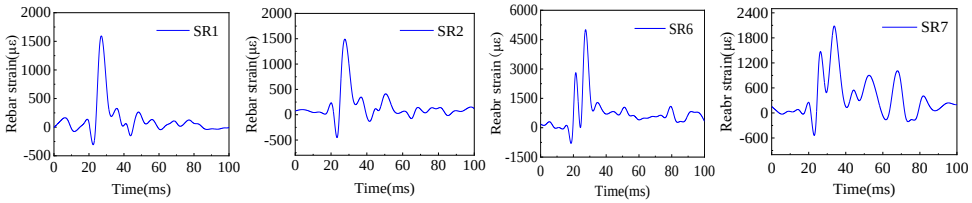

(**a**) SR1 (**b**) SR2 (**c**) SR6 (**d**) SR7

Figure 13. Measured rebar strain of specimen PCG.

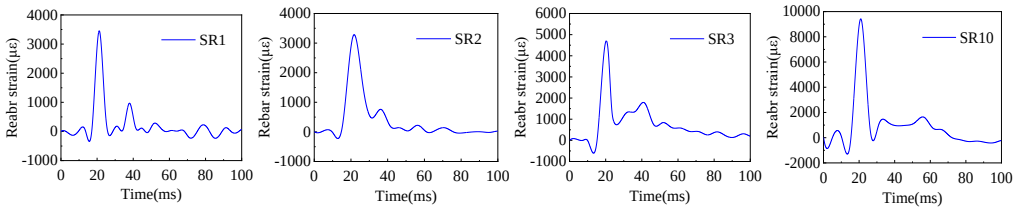

(**a**) SR1 (**b**) SR2 (**c**) SR3 (**d**) SR10

Figure 14. Measured rebar strain of specimen PCGR.

2.3.5. Vertical Acceleration

Figure 15 shows the temporal evolution curves depicting the vertical acceleration at the center of the baseplate in box chamber 2 for all specimens. The acceleration reaches its peak 42 ms after detonation, followed by oscillation and a gradual decay to zero. The recorded peak accelerations for specimens G, PCG, and PCGR were 36.5 km/s^2, 10.4 km/s^2, and 48.44 km/s^2, respectively. Specimen PCG showed a 71.4% reduction in peak acceleration compared to G, owing to the protective effect of the polyurea coating, which mitigated the blast shockwave and decreased vertical acceleration at the baseplate. In contrast, the peak acceleration for PCGR rose by 366.3% compared to PCG under repeated explosive loads. This is attributed to the damage and defects formed in the box girder after the first explosion, which weakened its blast resistance. Furthermore, a comparison of specimens G, PCG, and PCGR indicates that the acceleration curve for specimen G exhibits the largest oscillation amplitude, which further validates the capability of the polyurea coating for reducing explosive shockwaves, thereby enhancing the overall stability of the structure.

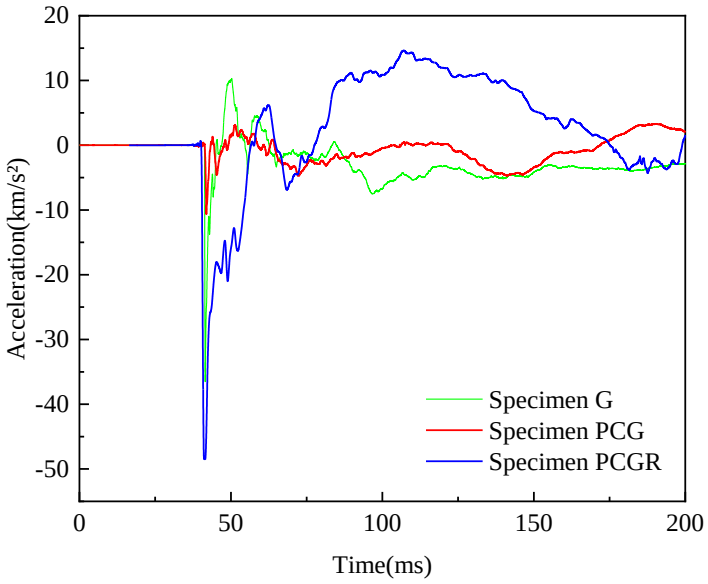

Figure 15. Test results of vertical acceleration of the baseplate of chamber 2.

3. Numerical Simulation and Validation

3.1. Finite-Element Model of Box-Girder Segment

A solid model of the box girder was constructed using SolidWorks and subsequently imported into HyperMesh for mesh generation. In the model, the concrete and polyurea were modeled using Solid164 solid elements, while the reinforcement was modeled using BEAM188 elements. The concrete material was defined using the *MAT_CONCRETE_DAMAGE_REL3 keyword in LS-DYNA, the reinforcement using the *MAT_PLASTIC_KINEMATIC keyword, and the polyurea using the *MAT_PIECEWISE_LINEAR_PLASTICITY keyword. The coupling of degrees of freedom between concrete and reinforcement was achieved using the CONSTRAINED_BEAM_IN_SOLID keyword in LS-DYNA. Shared

nodes were applied between the concrete and polyurea without considering interface debonding. As an example, the finite-element model for specimen PCG is illustrated in Figure 16. Explosion loads were applied using the *LOAD_BLAST_ENHANCED (LBE method) and *LOAD_SEGMENT_SET keywords in LS-DYNA. The explosion center was positioned 0.4 m directly above the center of the second box chamber, with a TNT equivalent of 3 kg, corresponding to a scaled distance of 0.31 m/kg^1/3. Based on observations from the blast test results of specimen G, no sliding or separation occurred between the support and the baseplate of the box girder. In the numerical simulation, the nodes between the baseplate of the box girder and the support were connected with shared nodes, and the bottom of the support was set as fully constrained. Considering both mesh accuracy and computational efficiency, the mesh size for the concrete and reinforcement was set to 30 mm [30].

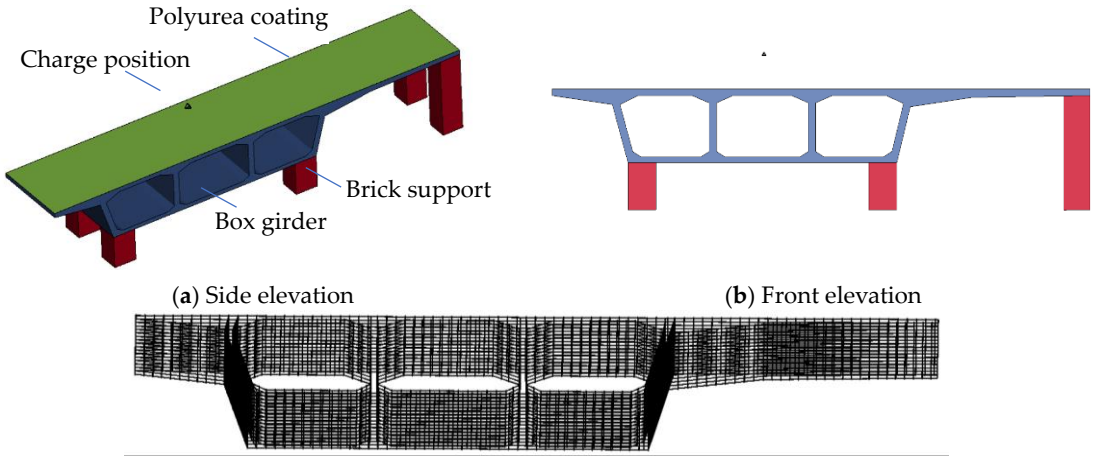

Figure 16. FEM of girder specimen PCG.

3.2. Material Parameters

The *MAT_CONCRETE_DAMAGE_REL3 constitutive model is used to simulate concrete, which is suitable for simulating the mechanical behavior of concrete under high strain rates and large deformations [33] and can define failure through erosion algorithms [34]. The material parameters of concrete are shown in Table 2.

Table 2. Material parameters of concrete.

Parameter	ρ/(kg/m^3)	A_0/GPa	RSIZE	UCF	LCRATE
Value	2320	-24.25×10^{-3}	39.37	1.45×10^{-4}	-1

The *MAT_PLASTIC_KINEMATIC constitutive model is widely used to simulate the dynamic mechanical behavior of steel bars under high-stress conditions. This model not only considers the strain rate effect of rebars in extreme environments such as explosive loads but also describes the failure mechanism during their plastic deformation process. The specific material parameters of steel bars are shown in Table 3.

Table 3. Material parameters of rebar.

Parameter	ρ/(kg/m^3)	E/GPa	ν	σ_Y/GPa	β	C	P	ε_F	VP
Value	7800	2	0.3	0.468	0	40	5	0.1	0

The hyperelastic constitutive model *MAT_PIECEWISELINEAR_PLASTICITY was employed to simulate polyurea, with failure criteria defined by a combination of fracture

strain and erosion algorithms. The strain-rate sensitivity of polyurea was accounted for using the Cowper–Symonds model [35], and the specific material parameters are detailed in Table 4.

Table 4. Material parameters of polyurea.

Parameter	ρ/(kg· m^{-3})	E/Pa	ν	σ_Y/Pa	E_t/Pa	β	C	P	ε_F	VP
Value	1020	2.3×10^8	0.4	6×10^6	3.5×10^6	0	98.2	4.5	0.85	0

In order to accurately simulate the good connection relationship between concrete and support in the experiment, the *MAT_JOHNSON_HOLMQUIST_CONCRETE constitutive model was used to simulate brick masonry material support and the joint with concrete [30]. The specific parameters are detailed in Table 5.

Table 5. Material parameters of brick support.

Parameter	ρ/(kg·m^{-3})	E_t/GPa	A	β	C	N	σ_Y/GPa	T/GPa	ε_F
Value	1986	5.18	0.63	1.56	0.0054	0.826	7.5×10^{-2}	6×10^{-3}	0.01

3.3. Model Validation

The comparison between the damage patterns of the specimens obtained from the 30 mm mesh size model and the simulated results is depicted in Figures 17–19. As shown in the figure, the dimensional errors of the spalling area on the underside of the top plate of Chamber 2 for specimen G are −2.90% in the short direction and −5.03% in the long direction. For specimen PCG, the errors are −11.8% and −11.3%, respectively, while for specimen PCGR, the errors are −0.32% and 7.96%. The possible reasons for these discrepancies include uneven concrete casting and variations in the mass of the explosive. In summary, the simulated perforation and indentation on the top plate closely match the experimental findings [30].

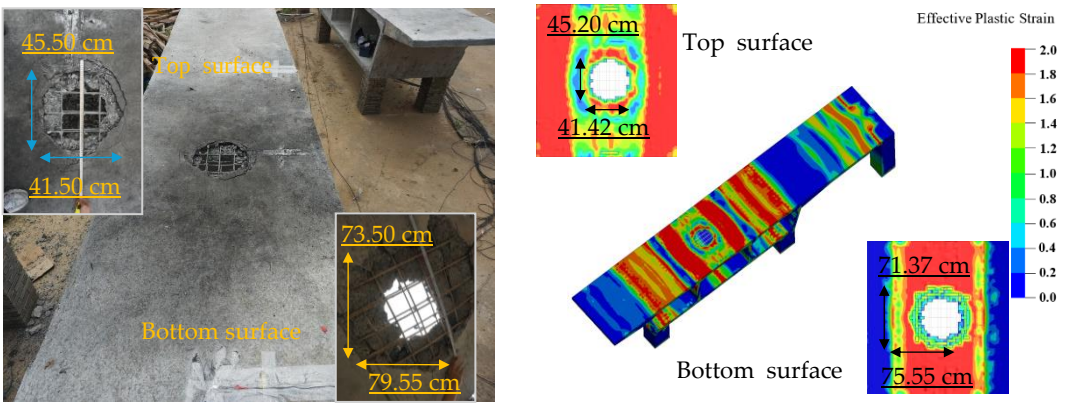

(**a**) Result of test (**b**) Result of simulation

Figure 17. The damage patterns of experimental and simulated results for specimen G.

The comparison of the experimental and simulated temporal evolution curves for vertical displacement and acceleration response at the central point of the baseplate in box chamber 2 of the specimen, as presented in Figure 20. For specimen G, the peak vertical displacement and peak acceleration deviations compared to test results are 10.59% and 15.00%, respectively. For specimen PCG, the deviations are −11.73% and −4.20%, while for specimen PCGR, the deviations are −6.66% and −8.62%, respectively. These results suggest that the failure behaviors and dynamic reactions of the specimens G, PCG, and PCGR in the numerical simulations closely align with the experimental results, underscoring the reliability of the finite element model and the simulation method.

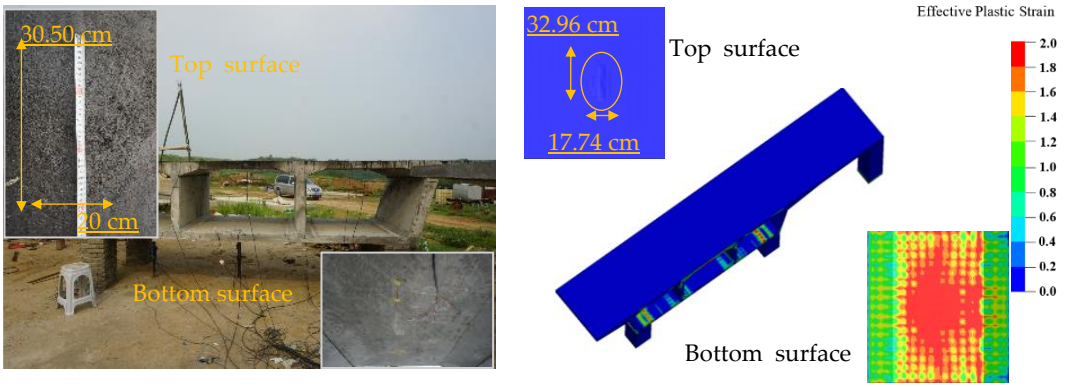

(**a**) Result of test (**b**) Result of simulation

Figure 18. The damage patterns of experimental and simulated results for specimen PCG [30].

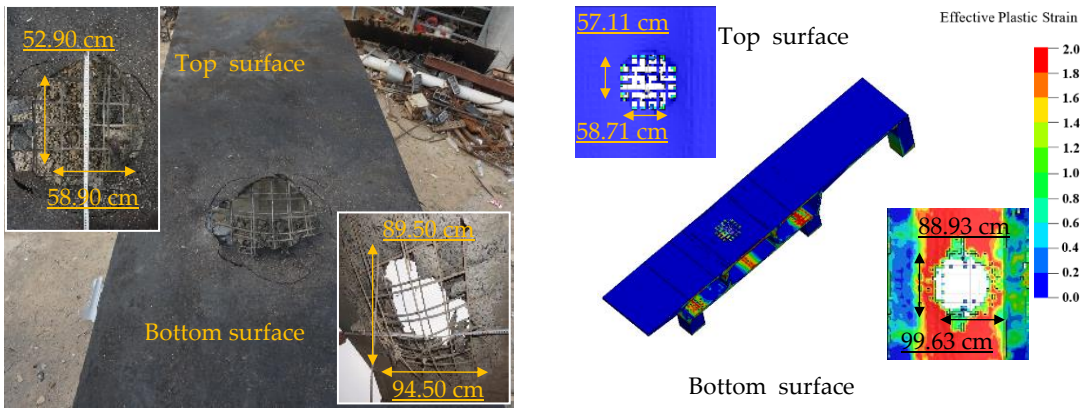

(**a**) Result of test (**b**) Result of simulation

Figure 19. The damage patterns of experimental and simulated results for specimen PCGR.

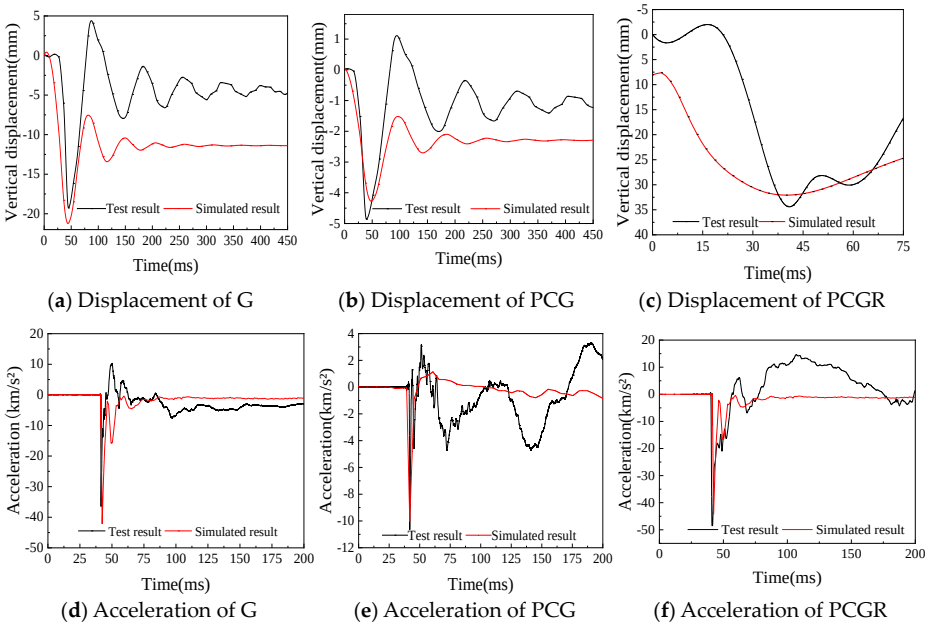

(**a**) Displacement of G (**b**) Displacement of PCG (**c**) Displacement of PCGR

(**d**) Acceleration of G (**e**) Acceleration of PCG (**f**) Acceleration of PCGR

Figure 20. Experimental and simulated data for vertical displacements and accelerations of the specimens.

4. Study on the Blast Resistance of Ultra-Wide Concrete Twin-Edge Box Girders Coated with Polyurea

4.1. Finite-Element Model of Ultra-Wide Concrete Twin-Edge Box Girder

4.1.1. Project Overview

Based on the engineering background of the Hunan Road Bridge in Liaocheng, Shandong Province [36], this structure is a suspension bridge consisting of spans measuring 53 m + 112 m + 53 m, featuring twin towers and dual cable planes. The main girder consists of a prestressed concrete twin-box section, with the two box girders unified by internal cantilevers and crossbeams. The main towers feature an H-shaped configuration with solid rectangular cross-sections. A total of 37 pairs of suspension cables are employed across the bridge: 8 pairs for each side span and 21 pairs for the main span. The suspension cables are spaced at regular intervals of 5 m. The concrete has a specified strength grade of C50, while the reinforcing steel is rated at HRB400. The bridge's overall configuration is illustrated in Figure 21.

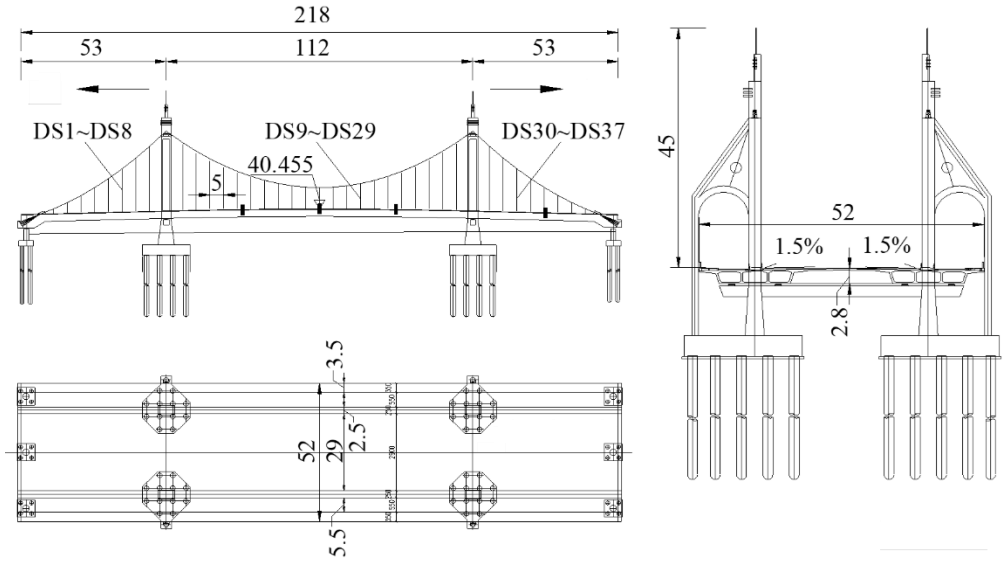

Figure 21. Overall bridge layout (units: m).

The main girder of the Hunan Road Bridge is a prestressed concrete twin-edge box girder, cast in situ using C50 concrete. The half-width girder consists of a single-box, three-cell configuration, symmetrical along the road centerline, with a height of 2.8 m at the centerline. The thicknesses of the top plate, baseplate, and web are 24 cm, 22 cm, and 35 cm, respectively. The main girder is reinforced with transverse and longitudinal prestressing tendons. The tendons are composed of high-strength, low-relaxation steel strands, each comprising 12 wires of 15.2 mm diameter strands, with a standard tensile strength of 1670 MPa. The structural layout of the half-width girder is shown in Figure 22.

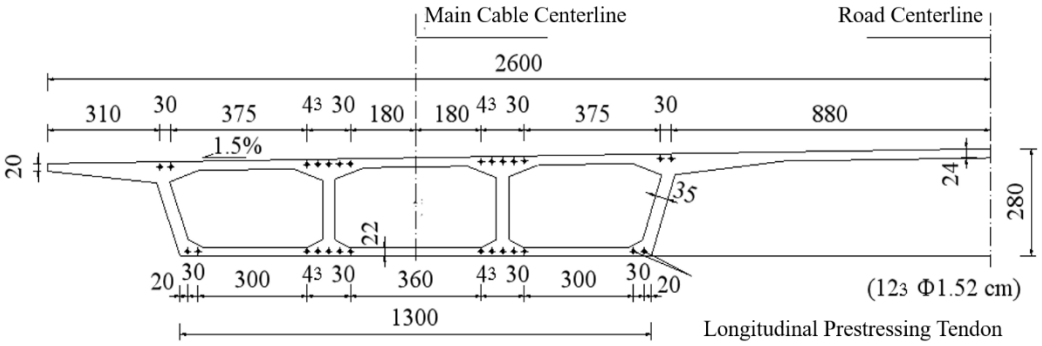

Figure 22. Structural layout of half-width main girder (Unit: cm).

4.1.2. Refined Finite-Element Model

The modeling approach, material characteristics, and blast load application for the concrete twin-edge box girder coated with polyurea follow the simulation method outlined for the blast response of the box-girder specimen as discussed in Section 2.3. Due to the 5 m spacing between hangers on the Hunan Road Bridge, connected to the lower part of each transverse diaphragm, a comparative analysis was performed to assess the blast-response distribution along the transverse direction of the box girder. Specifically, the analysis targets scenarios where the blast epicenter is positioned at the midpoint of each chamber, the web, and the central connection section (i.e., the T-beam section) to evaluate the non-uniformity of the response distribution. To minimize the influence of continuous transverse diaphragms along the girder's transverse direction, three 5 m-long segments of the box girder were chosen for the study. The full length of the modeled box girder prototype in the longitudinal axis is 15 m, with the detailed finite-element model shown in Figure 23.

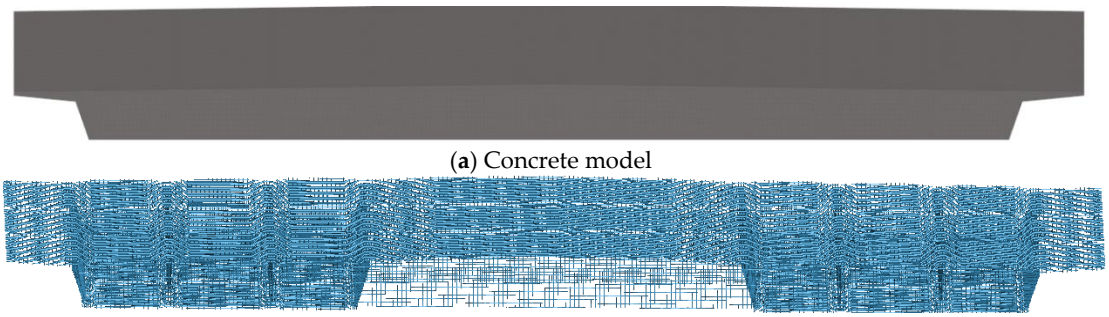

(**a**) Concrete model

(**b**) Rebars model

Figure 23. Finite-element model of the prototype ultra-wide concrete twin-edge box girder segment.

Solid164 elements were employed to represent both the concrete and polyurea materials, while BEAM188 elements were used for the rebars. The nodes of the concrete and polyurea elements were shared, and interfacial debonding was not considered. The relationship between the concrete and the rebars was defined using the *CONSTRAINED_BEAM_IN_SOLID keyword in the LS-DYNA software, and the effects of prestressing tendons were not considered. Both longitudinal ends of the twin-edge box girder were fully constrained. Based on the model validation in Section 3.3 and the findings of other scholars [37,38], a mesh size of 200 mm was adopted for computational accuracy and efficiency. The number of concrete elements totaled 127,416, and the number of rebar elements totaled 171,792.

4.2. Parametric Analysis

4.2.1. Analysis of the Impact of Different Scaled Blast Distances

This study examines the impact of close-range explosion shock waves on polyurea-coated ultra-wide concrete twin-edge box girders. The explosions considered typically involve car bombs or the detonation of fireworks and chemical hazardous materials transported on bridge decks, with their blast power equivalent to TNT charges applied to the bridge structure.

According to the FEMA 426 manual [39], based on common vehicle types and capacities, a large truck is typically capable of transporting at least 10,000 pounds (around 4536 kg) of TNT-equivalent explosives. Vans and smaller passenger vehicles are able to transport between 500 and 4000 pounds (roughly 227 to 1814 kg) of TNT equivalent. Drawing on the "Terminology and Definitions of Automobile and Trailer Types", Kong [40] classified common vehicles into five categories based on loading capacities: standard passenger cars, crossover vehicles, multi-purpose vehicles, minibuses, and box trucks. Due to strict national military security regulations on explosives, the equivalent quantity of common industrial explosives is reduced by a factor of 0.5. Thus, the TNT equivalent range for car bombs is set between 100 and 1000 kg.

In this study, five TNT-equivalent charge weights were selected for finite element simulations: 100 kg, 200 kg, 300 kg, 400 kg, and 500 kg. The specific experimental conditions are shown in Table 6.

Table 6. Blast conditions for varying charge weights.

Specimens	Condition	TNT Equivalent/kg	Blast Position		Blast Height/m	Scaled Distance/m/kg$^{1/3}$
			Transverse Direction	Longitudinal Direction		
PG/PPCG	1	100	Center of the top plate of box chamber 2	Mid-span	1	0.215
	2	200				0.171
	3	300				0.149
	4	400				0.136
	5	500				0.126

The damage patterns of the top plate of the prototype box girder segment before and after polyurea coating, under different scaled blast distances, are shown in Figure 24, with three measured dimensions of the top plate breach provided in Table 7. When the blast load impacts the top plate of the box girder, stress and strain within the concrete elements increase rapidly. As the blast shock wave persists, stress and strain in the concrete progressively reach their limits, leading to localized perforations in the top plate. As the TNT equivalent increases from 100 kg up to 500 kg, the length of the breach along the long edge of the uncoated PG specimen increased from 1.210 m to 2.429 m, and along the short edge from 1.361 m to 2.540 m. For the polyurea-coated PPCG specimen, the breach length along the long edge grew from 1.613 m to 2.829 m, and along the short edge from 1.755 m to 2.928 m. This indicates that the PPCG specimen with the polyurea coating exhibited relatively larger breach dimensions under the same blast load. The reason for this is that the polyurea-coated structure effectively absorbs and disperses the energy generated by the blast, converting more kinetic energy into fracturing energy on the top plate, thus resulting in larger breaches [30]. In the effective plastic strain contour diagrams shown in Figure 20, the area immediately below the blast center for both the PG and PPCG specimens is colored red, indicating a region of localized high strain, which suggests that damage is more severe in areas closer to the blast center. As the TNT charge increases, the breach area in the concrete enlarges, damage to the top plate worsens, and minor spalling occurs in the baseplate and web concrete. Additionally, the extent of the high-strain region immediately below the blast center expands.

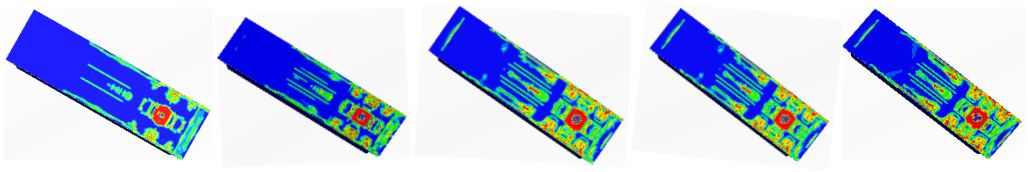

100 kg 200 kg 300 kg 400 kg 500 kg

(**a**) Specimen PG

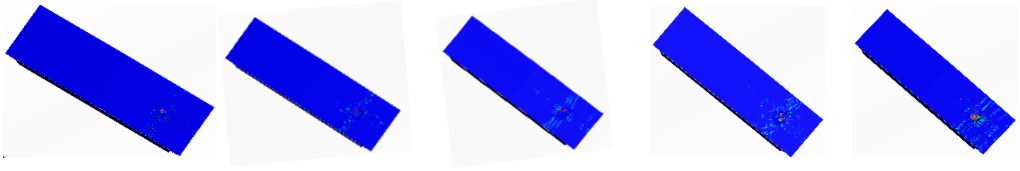

100 kg 200 kg 300 kg 400 kg 500 kg

(**b**) Specimen PPCG

Figure 24. Damage patterns of prototype box girder segments before and after polyurea coating under different scaled blast distances.

Table 7. Length of concrete spall on the top plate of box girder coated with polyurea segments under different charge amounts.

Specimens	TNT Equivalent/kg	Charge Position	Blast Heigh/m	Breach Length/m	
				Transverse Direction	Longitudinal Direction
PG	100	Middle of the top plate in box chamber 2	1	1.205	0.964
	200			1.609	1.756
	300			2.015	2.141
	400			2.026	2.146
	500			2.412	2.149
PPCG	100	Middle of the top plate in box chamber 2	1	1.613	1.755
	200			2.014	2.151
	300			2.620	2.535
	400			2.819	2.546
	500			2.829	2.928

Figure 25 shows the stress–time history curves for concrete elements at four locations under condition 1: the T-beam quarter-span, the middle of the top plate in box chamber 1, box chamber 3, and the outer cantilever section. The figure illustrates that the stress variation trend remains consistent at each point regardless of polyurea application, suggesting that polyurea affects only the peak stress, not the overall trend. For the uncoated specimen (PG), peak stresses are 8.73 MPa, 13.77 MPa, 13.28 MPa, and 6.61 MPa, while for the polyurea-coated specimen (PPCG), they are 4.75 MPa, 9.91 MPa, 10.68 MPa, and 5.62 MPa. These results show that polyurea significantly reduces peak stress at all locations. Peak stress reductions are 45.59%, 28.03%, 19.58%, and 14.98%, respectively. These findings confirm that the polyurea coating effectively reduces peak stress in concrete structures under blast loading, especially at the T-beam quarter-point, where the stress reduction is most pronounced. Moreover, peak stresses increase with proximity to the blast center. This suggests that the blast shockwave impact diminishes as the distance from the blast center increases. As the shockwave propagates outward, it sequentially reaches different points, producing peak stresses at each location. In summary, polyurea significantly reduces peak stress in concrete structures subjected to blast loading, especially at locations near the blast center.

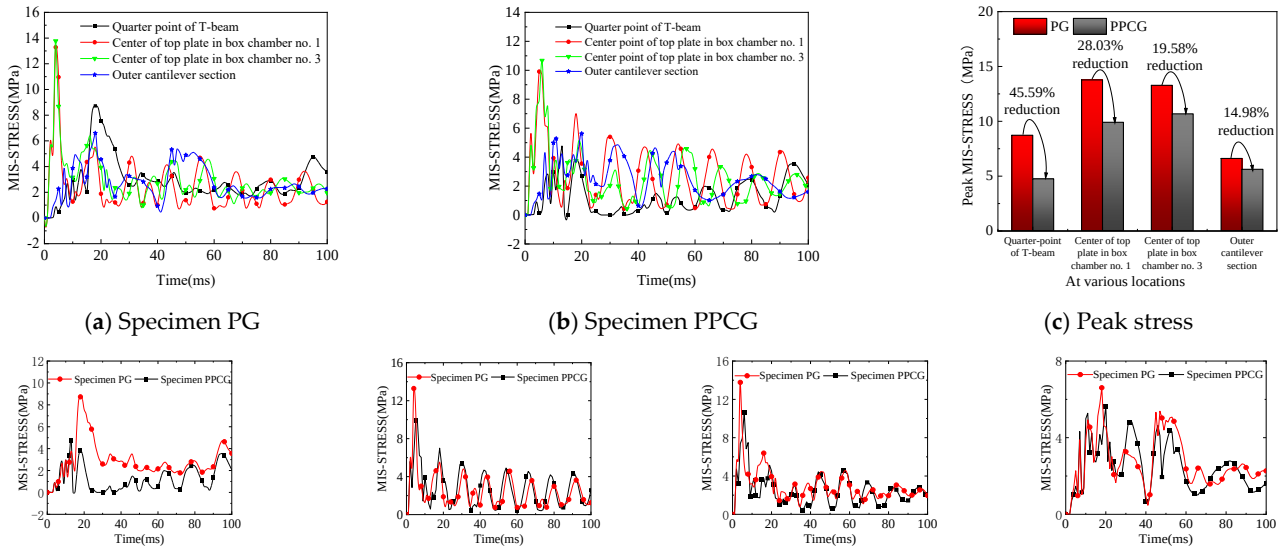

(**a**) Specimen PG (**b**) Specimen PPCG (**c**) Peak stress

(**d**) Quarter-point of T-beam (**e**) Center of box chamber 1 (**f**) Center of box chamber 3 (**g**) Outer cantilever section

Figure 25. Temporal evolution curve of concrete stress of the ultra-wide box girder (condition 1).

The time–history curves of concrete stress at the top-plate center of box chamber 1 under different scaled distances are shown in Figure 26. When the blast height is constant,

the peak stress in the top plate of box chamber 1 increases with the explosive charge, resulting in a reduced scaled distance. This demonstrates the concrete structure's sensitivity to explosive charges, where higher charges lead to increased peak stress. For the five different test conditions, the maximum stress values for specimen PG were 13.28 MPa, 18.22 MPa, 19.42 MPa, 22.77 MPa, and 24.29 MPa, respectively. In contrast, the maximum stress values for specimen PPCG were 9.91 MPa, 17.03 MPa, 18.61 MPa, 21.83 MPa, and 22.51 MPa, showing consistently lower values than those of specimen PG. The reduction in peak stress due to the polyurea coating was 25.43%, 6.53%, 4.17%, 4.13%, and 7.33%, respectively, indicating that polyurea effectively mitigates the peak stress in concrete structures under blast impact. Notably, stress reduction is more significant under lower explosive charges.

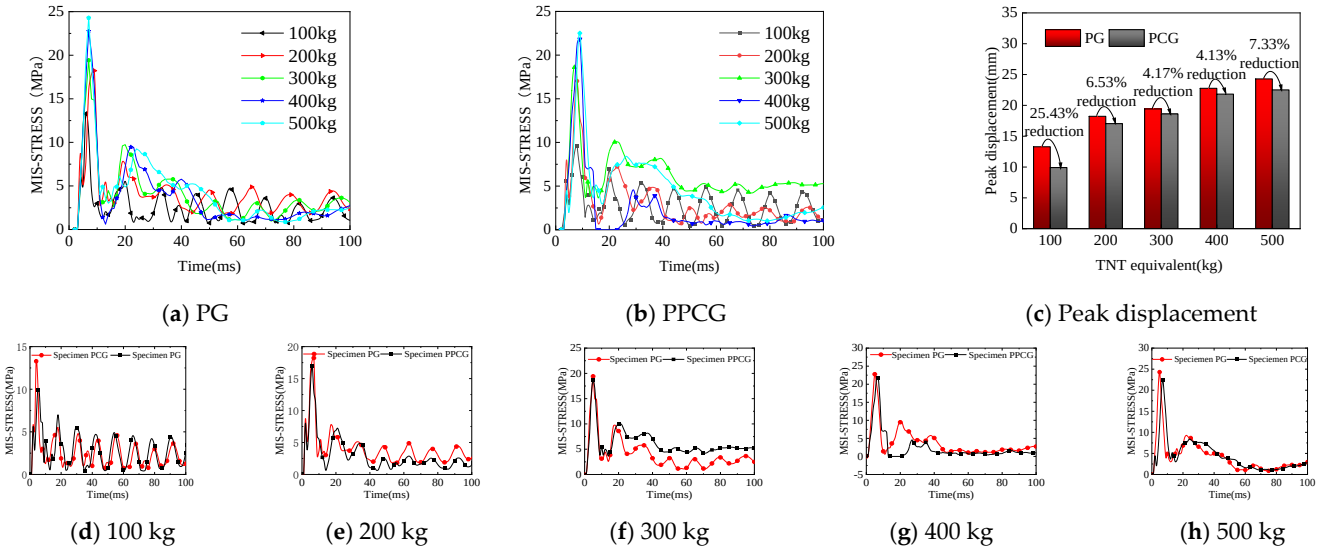

(**a**) PG (**b**) PPCG (**c**) Peak displacement

(**d**) 100 kg (**e**) 200 kg (**f**) 300 kg (**g**) 400 kg (**h**) 500 kg

Figure 26. Temporal evolution curves of concrete stress at the top-plate center of box chamber 1 under varying scaled blast distances.

The temporal evolution curves depicting the vertical shift of the baseplate directly beneath the blast center at varied scaled blast distances are depicted in Figure 27. As shown in the figure, under the impact of the blast shockwave, the vertical shift of the box girder rapidly reaches its highest point over a short duration before transitioning into a decay phase. The highest displacements observed in the baseplate under the blast zone for specimen PG under blast scenarios 1 to 5 are 6.99 mm, 8.82 mm, 12.41 mm, 17.92 mm, and 24.61 mm, respectively, while for Specimen PPCG, the corresponding maximum displacements are 5.63 mm, 8.53 mm, 11.53 mm, 14.61 mm, and 19.45 mm. These results indicate that the vertical shift of the girder grows progressively with increasing blast charge. Additionally, the proportional blast distance significantly affects both the damage and dynamic response of specimens PG and PPCG. Under blast scenario 4, specimen PPCG demonstrated superior protective performance coated with polyurea, reducing the peak displacement by 35.66% compared to specimen PG. This suggests that the application of polyurea coatings has a notable suppressive effect on reducing the vertical displacement of box girder structures under blast impact.

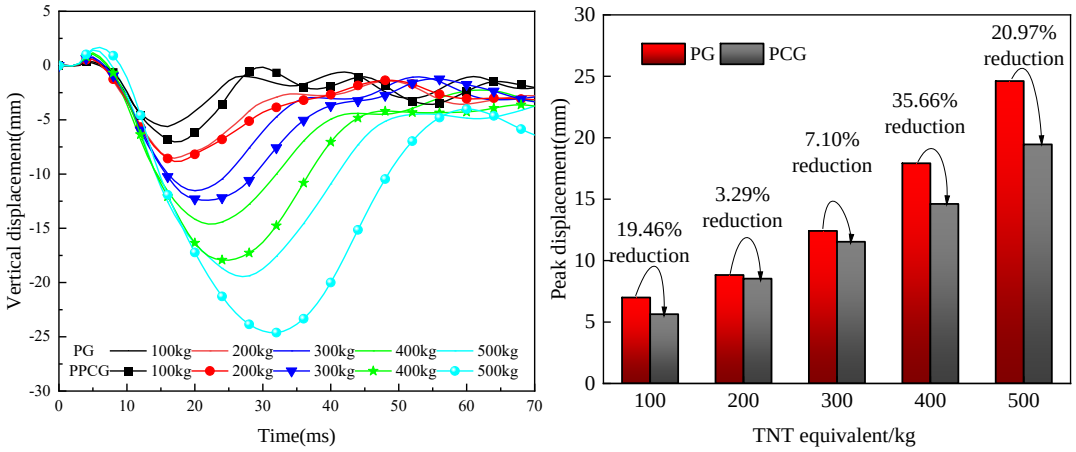

Figure 27. Vertical displacement time histories and peak curves of the baseplate under different TNT equivalents.

4.2.2. Analysis of the Impact of Different External Detonation Positions on the Box Girder

The primary girder of a bridge generally consists of a roadway, non-motorized lanes, bike paths, and pedestrian walkways. Considering the randomness of vehicle movement, this study examines the dynamic response and damage patterns of the primary girder in a bridge when subjected to explosive forces at various lateral positions. Detonation points along the width of the girder span include critical areas such as the roadway centerline, the connection between box chamber 1 and T-beam, and the web regions between box chambers. Additional blast locations involve the central points of the top plates in chambers 1, 2, and 3, along with the cantilever section. The blast conditions, with a TNT equivalent of 200 kg and the blast center placed 1 m above the top plate, are visually presented in Figure 28. Full details can be found in Table 8.

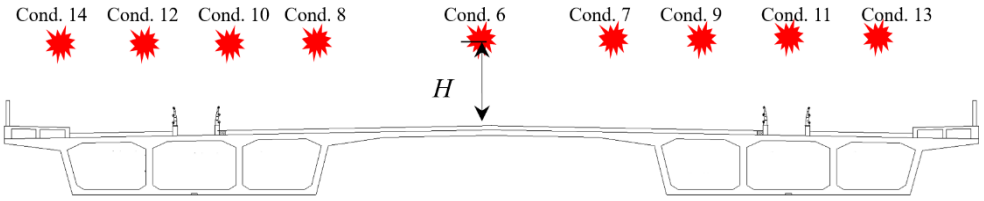

Figure 28. Schematic diagram of blast points across the transverse direction.

Table 8. Blast-response calculation conditions for prototype box-girder segments under different transverse blast locations.

Specimen	Condition	TNT/kg	Blast Charge Position		Blast Height/m	Scaled Standoff Distance/m/kg$^{1/3}$
			Transverse Direction	Longitudinal Direction		
PG/PPCG	6	200	Centerline of the roadway	Mid-span	1	0.171
	7		Quarter-span of the T-beam			
	8		Web-connecting box chamber 1 and T-beam.			
	9		Top plate center in box chamber 1			
	10		Web section between box chambers 1 and 2			
	11		Top plate center in box chamber 2			
	12		Web section between box chambers 2 and 3			
	13		Top plate center in box chamber 3			
	14		Web-connecting box chamber 3 to the cantilever.			

The damage patterns of specimens PC and PPCG under loading conditions 6 through 14 are shown in Figure 29. The failure mode of specimen PC primarily consists of full penetration damage to the deck plate. In contrast, the failure of specimen PPCG shows

localized damage to the upper deck surface without penetration to the bottom surface. In specimen PC, the concrete at the back side of the deck plate suffers spalling, which is caused by the interaction of the blast wave on the front side and tensile stresses on the rear, resulting in a funnel-shaped breach. For specimen PPCG, the polyurea coating dissipates the blast energy, preventing spalling on the back-blast side and demonstrating protective efficacy. Damage to the deck plate is more significant when the explosion occurs above the web compared to the box chamber or T-beam sections. This is because when the explosion occurs above the web, the deck plate in specimen PC undergoes constrained deformation due to the web's reinforcing effect, which reduces its energy-absorption capacity. As a result, the deck plate experiences greater deformation and a subsequently larger damage area under blast loading. Compared to detonations in the center of the box chamber and the T-beam section, the constraint effect from a detonation above the web makes the deck plate more susceptible to impact and damage. In conclusion, the polyurea provides effective protection for the underside of the deck plate, mitigating damage to the bottom surface.

Based on the classification of ultra-wide box girder structures, the configurations are categorized into three types: box chamber center, T-beam sections, and web. A comparative analysis of these categories is provided below:

Based on the classification of ultra-wide box girder structures, the configurations can be categorized into three types: box chamber center, T-beam sections, and web. A comparative analysis of these classifications is provided below:

(1) Detonation above the center of the box chamber

When the blast is located above the midpoint of each box chamber, the temporal evolution curves illustrating the vertical shift of the baseplate in chambers 1 to 3 are shown in Figures 30–32. When the explosion originates at the box chamber center, the maximum vertical displacement values recorded at the baseplate just below the explosion point for specimens PG and PPCG are the highest. Specifically, under condition 9, the vertical shift measured at the center of the baseplate in chamber 1 of specimen PG reaches 9.15 mm; under condition 11, the peak in chamber 2 is 8.67 mm; and under condition 13, the peak in chamber 3 is 12.69 mm. For specimen PPCG, under the same conditions, the peak vertical displacement values are 8.72 mm for chamber 1 (condition 9), 8.45 mm for chamber 2 (condition 11), and 12.21 mm for chamber 3 (condition 13), indicating reductions of 4.70%, 2.54%, and 3.78%, respectively, compared to specimen PG. These results demonstrate that for both specimens PG and PPCG, as the distance from the explosion center shortens, the peak vertical displacement grows. The region immediately beneath the explosion point experiences the most intense impact from the blast wave, and, due to boundary effects, the vertical displacement response in chamber 3, located at the end of the main girder, is more pronounced. Following the application of polyurea coating, the vertical displacement measured at the baseplate right beneath the explosion point slightly decreases under identical conditions.

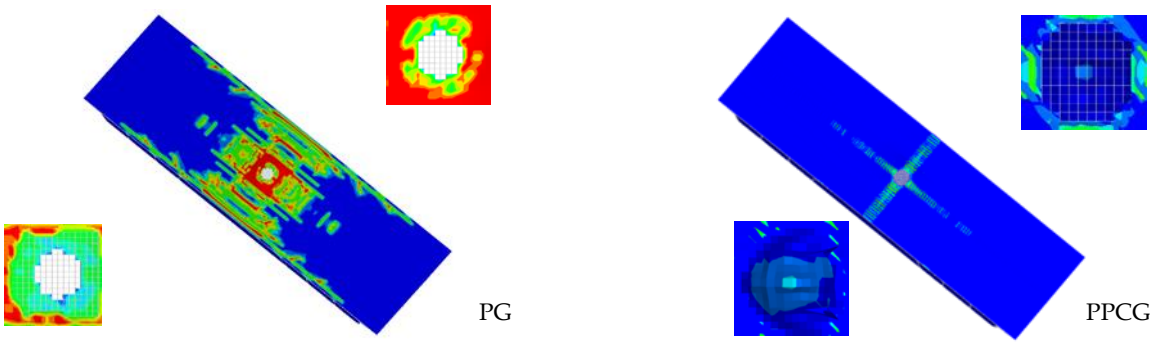

(**a**) Condition 6: Road centerline

Figure 29. *Cont.*

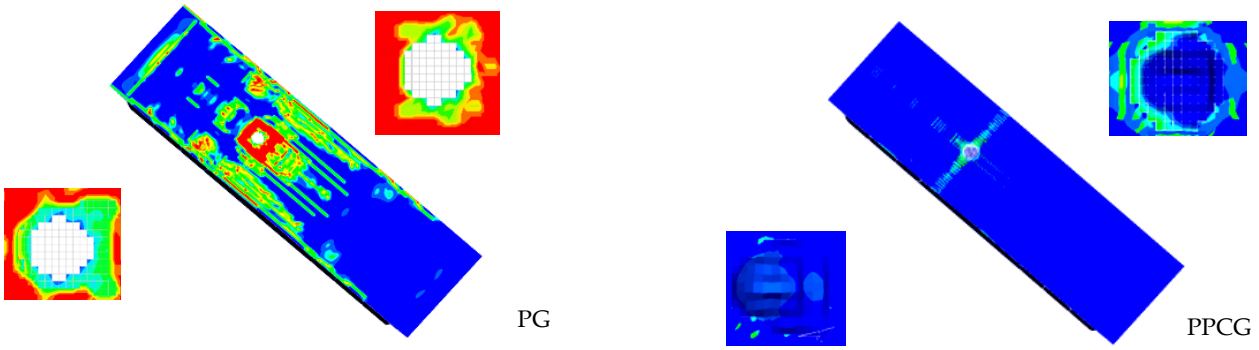

(**b**) Condition 7: The quarter-span along the T-beam section

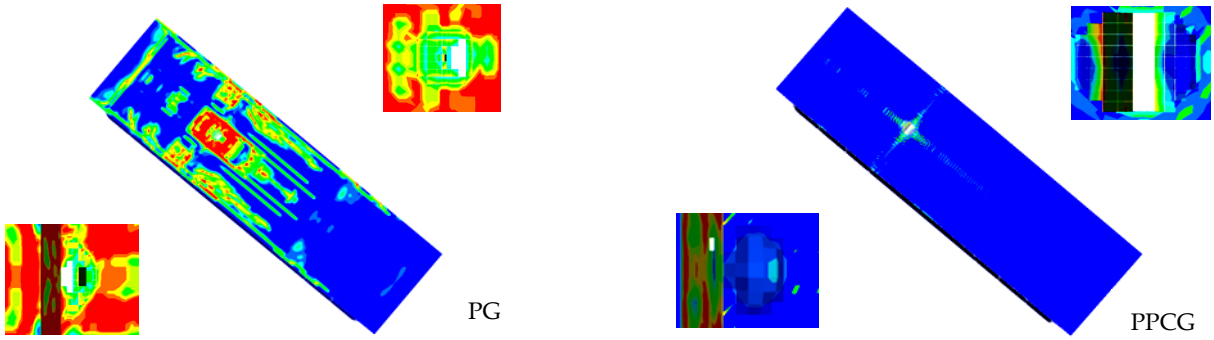

(**c**) Condition 8: The web located between box chamber 1 and the T-beam section

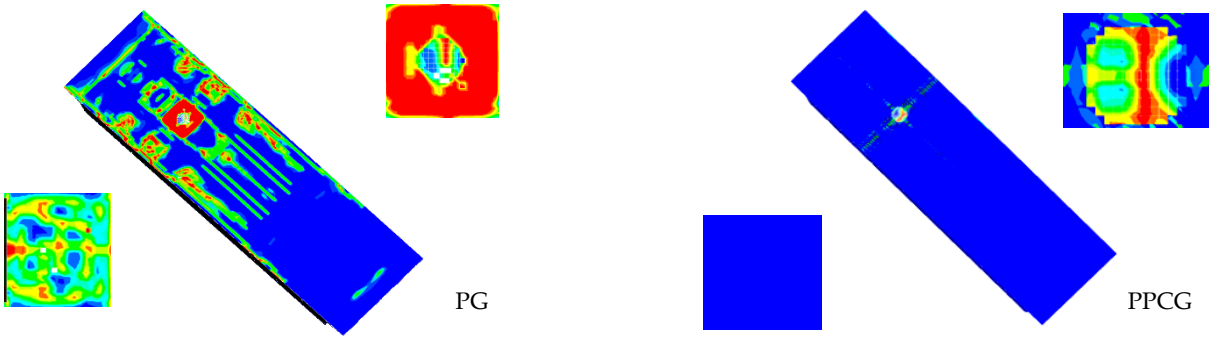

(**d**) Condition 9: Center of the top plate of box chamber 1

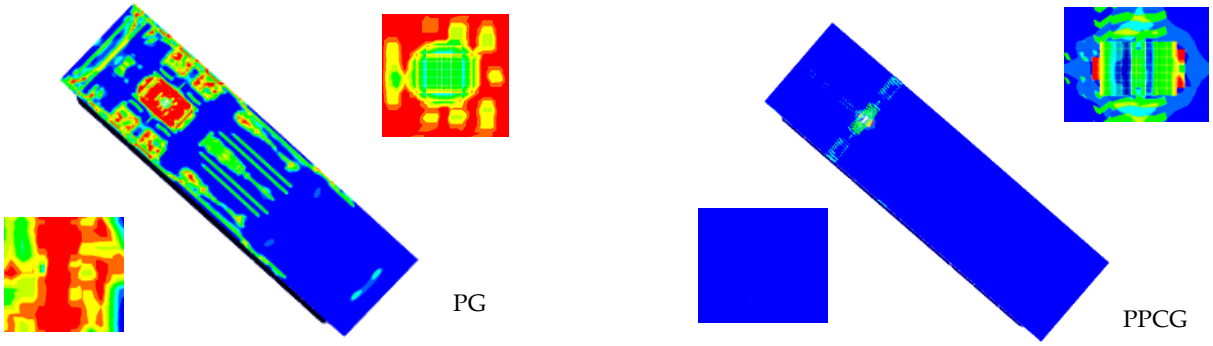

(**e**) Condition 10: The web positioned between chambers 1 and 2

Figure 29. *Cont*.

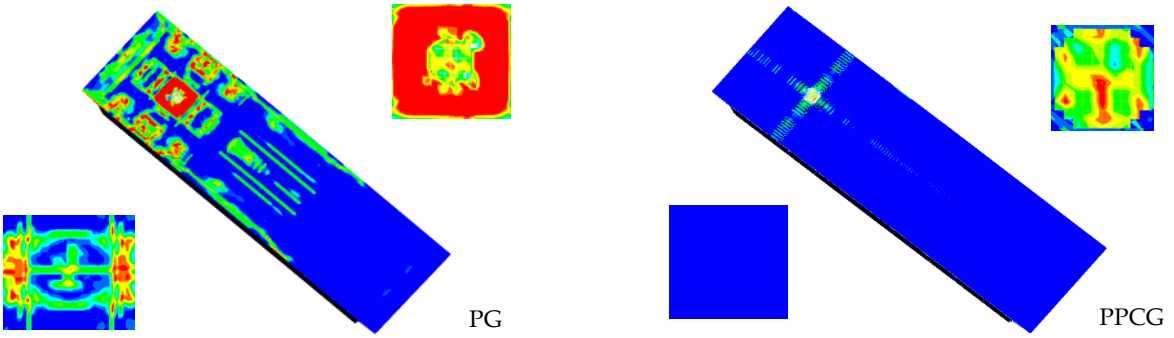

(**f**) Condition 11: Center of the top plate of box chamber 2

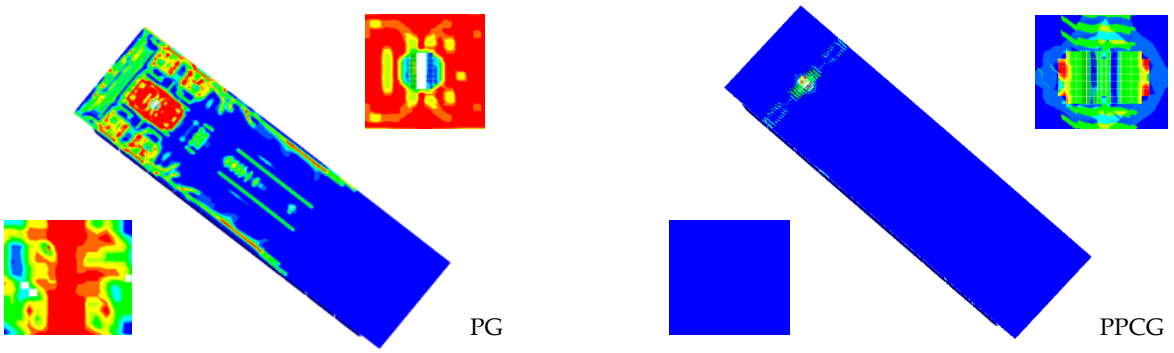

(**g**) Condition 12: The web connecting box chambers 2 and 3

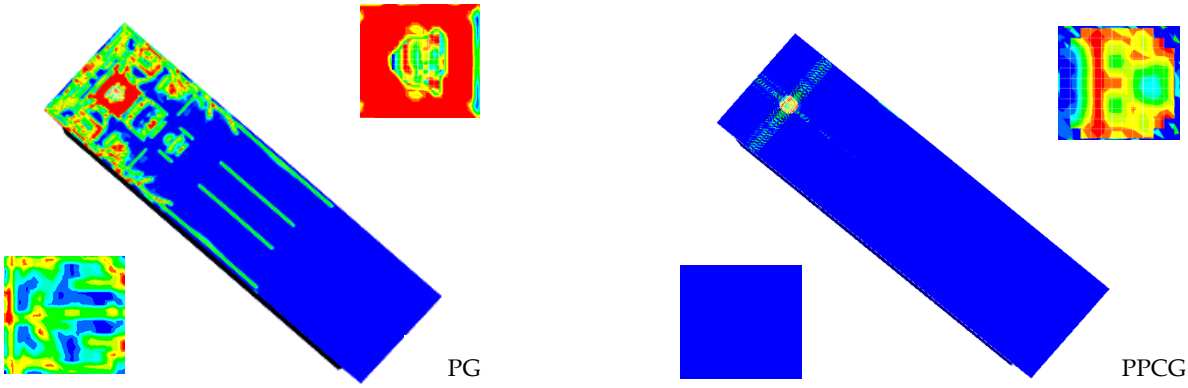

(**h**) Condition 13: Center of the top plate of box chamber 3

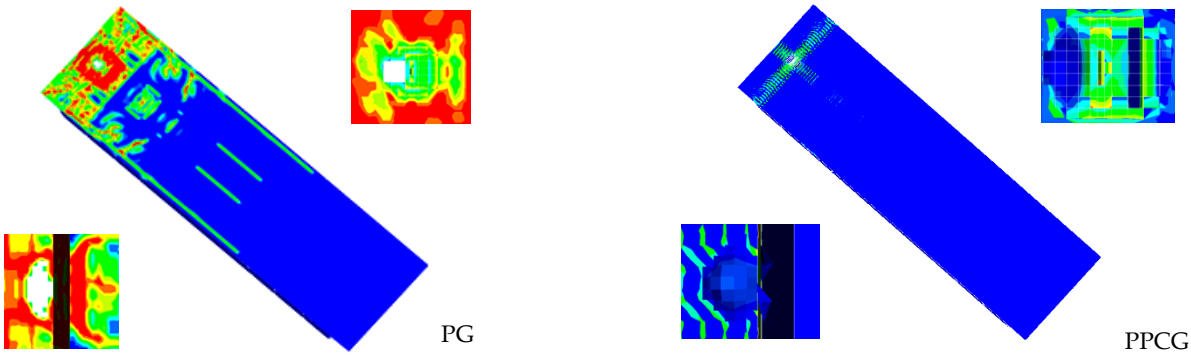

(**i**) Condition 14: The web linking chamber 3 to the outer cantilever section

Figure 29. Failure modes in conditions 6–14.

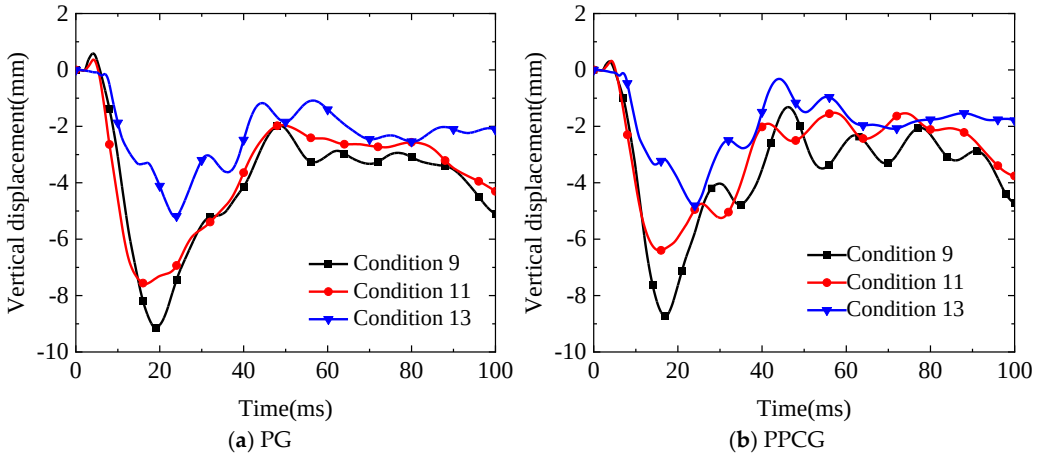

Figure 30. Temporal evolution curves of vertical displacement at the center of the baseplate in box chamber 1 under conditions 9, 11, and 13.

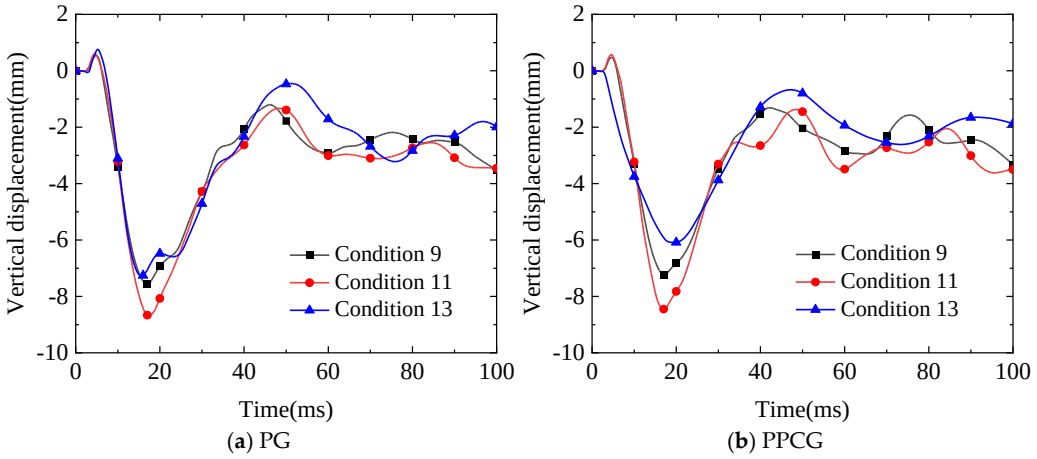

Figure 31. TNT equivalent of vertical displacement at the center of the baseplate in box chamber 2 under conditions 9, 11, and 13.

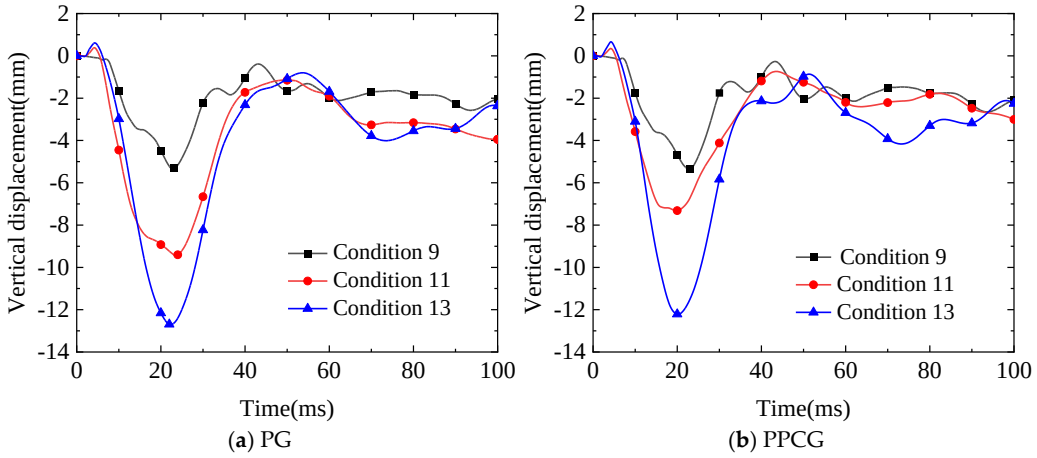

Figure 32. TNT equivalent of vertical displacement at the center of the baseplate of box chamber 3 under conditions 9, 11, and 13.

(2) Blast detonation above the webs

The temporal evolution curves of vertical displacement for the baseplates in chambers 1 to 3 subjected to blast conditions, with the detonation point above the web separating

the chambers, are shown in Figures 33 and 34. As observed, during condition 10, the highest vertical displacements of the baseplate in chambers 1 and 2 of specimen PG are 14.45 mm and 12.56 mm, respectively, while in specimen PPCG, the corresponding values are 13.43 mm and 11.03 mm. The peak displacements of specimen PPCG are reduced by 7.06% and 12.18%, respectively, compared to specimen PG. The vertical displacement patterns at the baseplate centers on either side of the web are consistent for specimens PG and PPCG, showing similar peak displacements. Notably, the application of polyurea significantly reduces the displacement in the longitudinal direction near the boundary. During condition 12, the maximum vertical shifts of the baseplate of chambers 2 and 3 of specimen PG are 11.21 mm and 17.36 mm, respectively, while in specimen PPCG, the corresponding values are 10.20 mm and 14.27 mm. Compared to specimen PG, the peak displacements of specimen PPCG are reduced by 9.01% and 17.80%, respectively. Both specimens PG and PPCG exhibit similar trends in the vertical shift at the baseplate centers on either side of the web. However, the displacement in the baseplate of chamber 3 exceeds that in chamber 2, likely because chamber 3 is located at the end of the main girder's cross-section, where the constraining effect is weaker. These results indicate that the response in each chamber is closely linked to the cross-sectional design and the boundary conditions of the ultra-wide box girder. The position of the chambers and their relative distance from the boundaries affect the intensity of the blast impact and the degree of restraint, thereby influencing the vertical shift of the baseplate. The closer the chamber is to the boundary, the more effective the polyurea layer is in reducing the peak vertical displacement. This is because the polyurea coating provides effective protection in regions near the boundary, effectively mitigating the peak vertical displacement of the baseplates.

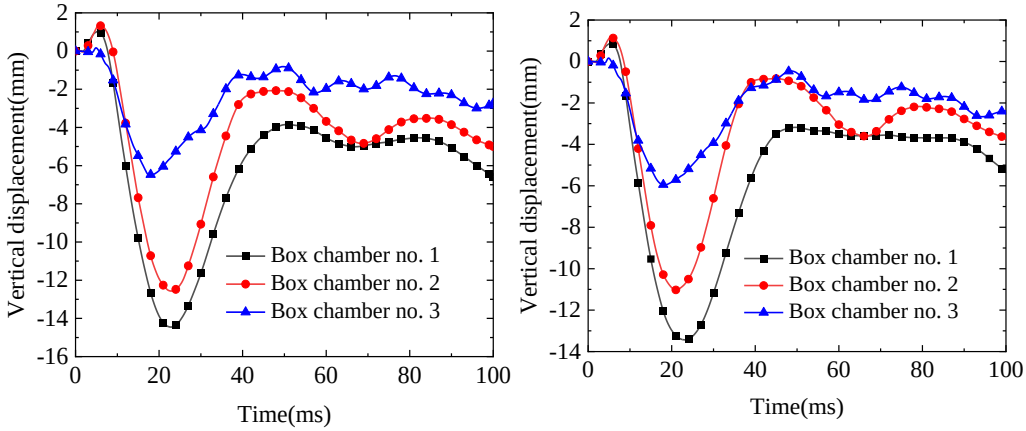

Figure 33. Temporal evolution curves of vertical shift at the baseplate center of the box chamber for condition 10.

(3) Distribution pattern of vertical displacement in ultra-wide box girders across the transverse direction

When the blast is located over the middle of the T-beam section, at the quarter-span, above the innermost web, over the center of the box girder, and above the outermost web, the temporal evolution curves of vertical displacement beneath the transverse diaphragms are shown in Figure 35. The vertical displacement trends for specimens PG and PPCG were generally consistent across various test conditions. Under test conditions 6, 7, 8, 11, and 14, the peak vertical displacements at the bottom of the transverse diaphragm for specimen PG were 12.82 mm, 10.07 mm, 9.67 mm, 6.08 mm, and 3.27 mm, respectively, while the corresponding peak vertical displacements for specimen PPCG were 12.26 mm, 9.84 mm, 9.46 mm, 5.97 mm, and 3.25 mm, respectively. Specimen PPCG exhibited reductions in peak displacements of 4.37%, 2.28%, 2.17%, 2.17%, and 0.61%, respectively, in comparison to specimen PG. Among these conditions, the highest peak vertical displacement observed at the bottom of the transverse diaphragm was in condition 6, with the explosion centered

over the middle of the T-beam section, followed by condition 7, where the explosion occurred at the quarter-span of the T-beam section. The lowest peak displacement was observed in condition 14, where the explosion was positioned between the web of the third box chamber and the outer cantilever section. The results indicate that the peak shift of the box girder just beneath the explosion epicenter, as well as the effectiveness of the polyurea coating in blast resistance, both decrease consistently from the middle of the T-beam section outward towards the outermost web. This indicates that the middle T-beam section is the weakest point in blast resistance for the polyurea-coated twin-chamber box girder. Overall, the specimen PPCG coated with polyurea exhibited improved blast-resistance performance across different test conditions, as evidenced by the relative reduction in peak vertical displacements at the bottom of the transverse diaphragm in comparison to the uncoated specimen PG.

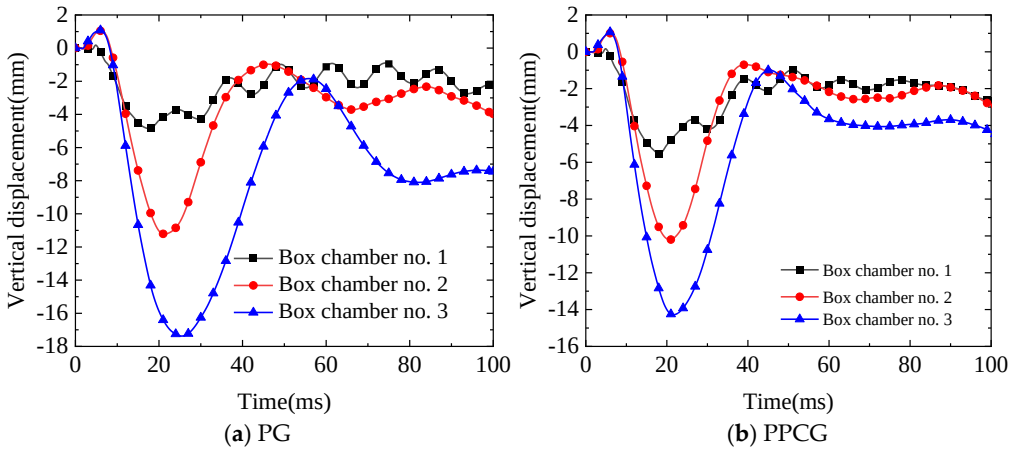

Figure 34. Temporal evolution curves of vertical shift at the baseplate center of the box chamber for condition 12.

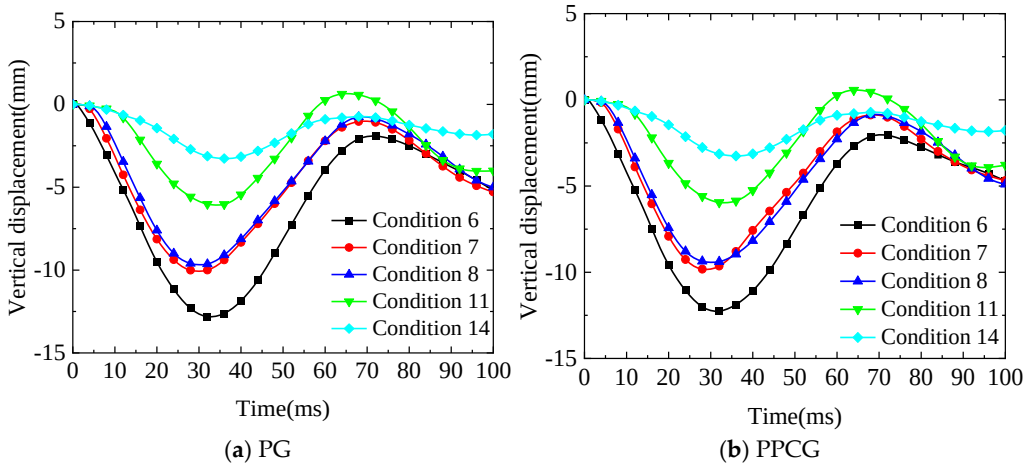

Figure 35. Temporal evolution curves at the bottom of the diaphragm beam near the area directly below the explosion center.

4.2.3. Analysis of the Impact of Different Repeated Explosion Patterns

(1) Single-point repeated detonation

As discussed in Section 2.3.2, the initial blast load causes localized damage to the reinforced concrete box girder and leads to material degradation focused on the explosion center. Under repeated blast loading, the box girder sustains progressively more severe damage. A comparative analysis was performed to investigate the failure characteristics of ultra-wide box-girder segments under both single and repeated explosion scenarios. Details of the calculation conditions are provided in Table 9.

Table 9. Single-point repeated detonation scenarios.

Specimen	Condition	Number of Blasts	Blast Charge Position		Blast Height/m	TNT Equivalent/kg	Scaled Standoff Distance/m/kg$^{1/3}$
			Transverse Direction	Longitudinal Direction			
PG and PPCG	15	First blast and second blast	Center of the top plate of box chamber 2	Mid-span	1	100	0.171
	16	First blast and second blast	Center of the top plate of box chamber 2	Mid-span	1	200	0.171

The comparison of damage patterns between repeated explosions and a single explosion on the ultra-wide box girder coated with polyurea is shown in Figure 36. As depicted in Figure 36a, after the initial 100 kg TNT blast, a through-hole appeared in the top plate center of chamber 2 of specimen PG, measuring 1.205 m along the long edge and 0.964 m along the short edge. After the second 100 kg TNT blast, the area of the through-hole increased to 2.220 m along the long edge and 2.544 m along the short edge. Similarly, in specimen PPCG, a through-hole appeared after the first 100 kg TNT blast, measuring 1.613 m along the long edge and 1.755 m along the short edge, and it was enlarged to 1.990 m by 1.734 m after the second blast. The shockwave passed through the hole, hitting the baseplate directly and causing concrete spalling on the rear face. The bending of both the transverse and longitudinal reinforcement bars around the perforation in the box girder increased, as did the permanent deformation of the bars. As shown in Figure 36b, under the condition described in Table 9 (200 kg single explosion), a through-hole formed at the center of the top plate of chamber 2 in specimen PG, measuring 1.609 m along the long edge and 1.756 m along the short edge, while the hole in specimen PPCG measured 2.014 m by 2.151 m. It can be concluded that compared to the 200 kg single explosion, both specimens PG and PPCG exhibited more severe damage under repeated explosions with two 100 kg charges, despite the same total charge. The top surface of the hole in specimen PPCG was smaller than that in PG, but the bottom surface hole in PPCG along the short edge increased significantly and was larger than in PG. This is because the energy-absorbing mechanism of the polyurea coating converts part of the internal energy into the crushing of the concrete.

From the comparison in Figure 36c,d, it can be observed that the same pattern holds when comparing two 200 kg repeated explosions with a single 400 kg explosion.

Figure 37 compares the temporal evolution curves of vertical shift at the center of the baseplate in the super-wide box girder subjected to repeated and single explosions. As shown in Figure 37a, under the first explosion of 100 kg on specimen PG, the peak vertical shift of the baseplate in chamber 2 was 6.83 mm, and under the second explosion of 100 kg, the peak displacement was 3.92 mm, resulting in a total displacement of 10.75 mm for both explosions. Under a single 200 kg explosion, the peak vertical displacement was 8.67 mm. For specimen PPCG, the peak vertical displacement was 5.66 mm under the first 100 kg explosion and 4.64 mm under the second explosion, with a total displacement of 10.30 mm. In contrast, the peak displacement under a single 200 kg explosion was 8.45 mm. Therefore, the increase in displacement under two 200 kg repeated explosions, compared to a single 400 kg explosion, was 19.34% for PG and 17.96% for PPCG. Under two 100 kg repeated explosions, the displacement decreased by 4.19% when comparing PG and PPCG specimens.

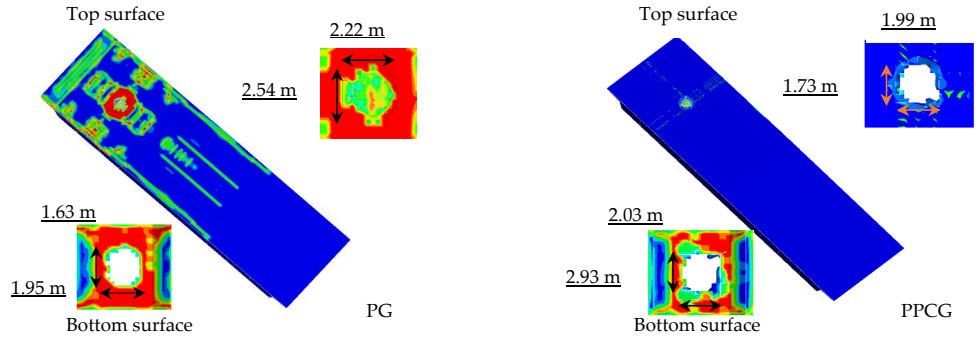

(**a**) Repeated explosion condition 15: 200 kg

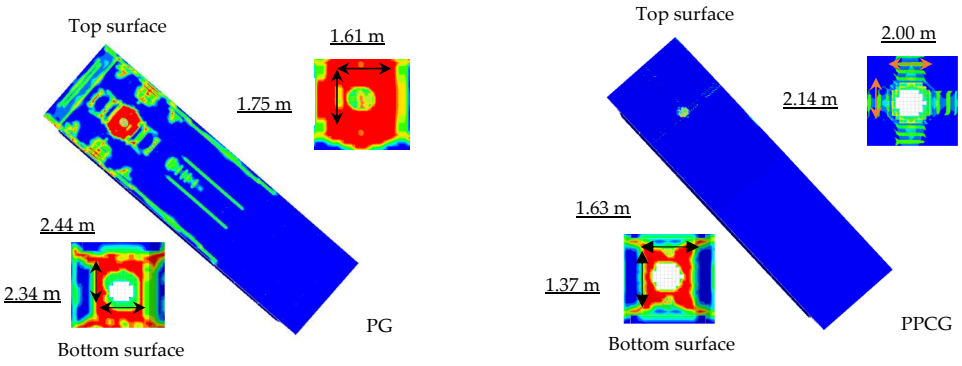

(**b**) Single explosion condition 16: 200 kg

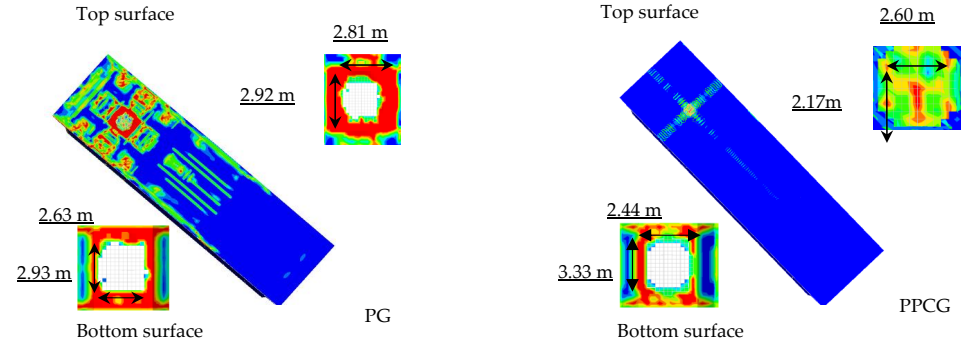

(**c**) Repeated explosion condition 16: 400 kg

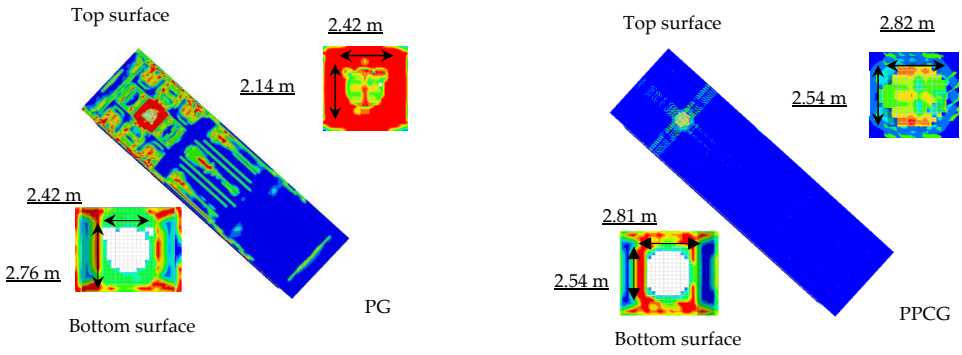

(**d**) Single explosion: 400 kg

Figure 36. Comparison of damage patterns in the ultra-wide box girder subjected to repeated and single blasts.

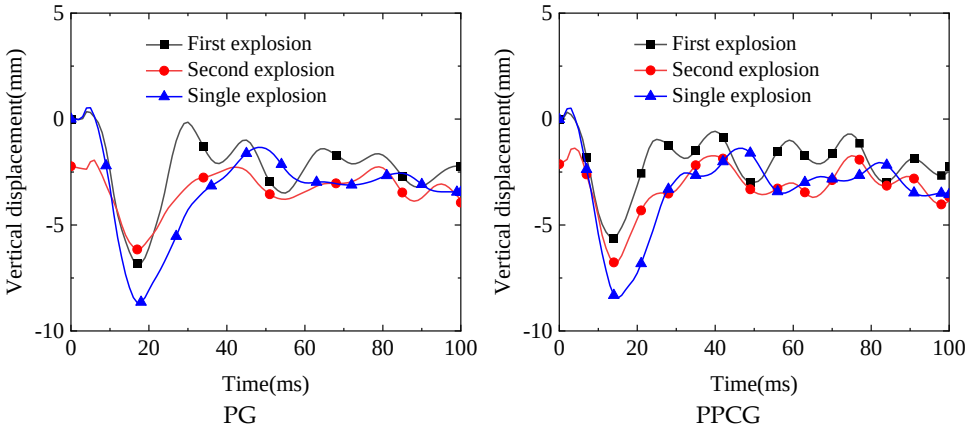

(**a**) Total TNT equivalent: 200 kg

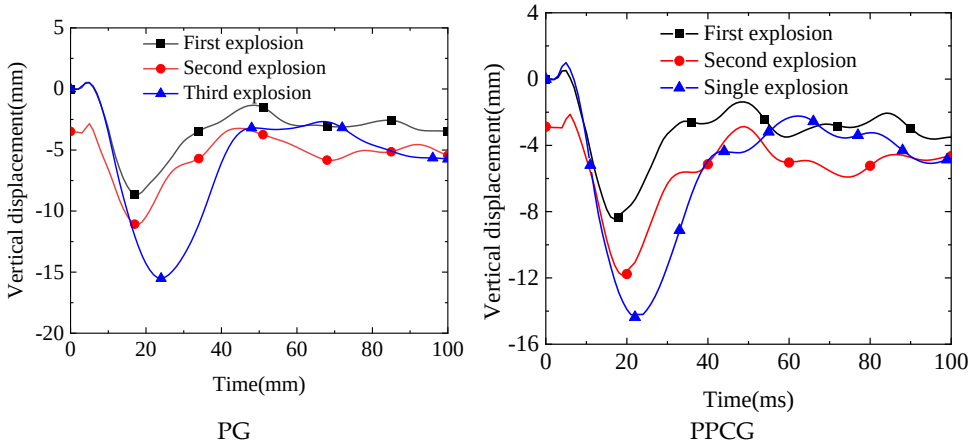

(**b**) Total TNT equivalent: 400 kg

Figure 37. Comparison of vertical-displacement time–history curves of ultra-wide box girder under repeated explosion and single explosion.

As shown in Figure 37b, the peak vertical displacement in chamber 2 of specimen PG under the first 200 kg explosion was 8.67 mm, and under the second explosion of the same charge, it was 7.61 mm, with a total displacement of 16.28 mm. Under a single 400 kg explosion, the peak displacement was 15.52 mm. For specimen PPCG, the peak vertical displacement was 8.45 mm under the first 200 kg explosion and 8.94 mm under the second explosion, resulting in a total displacement of 17.39 mm. The peak displacement under a single 400 kg explosion was 14.37 mm. Thus, compared with a single 400 kg explosion, the displacement increases for PG and PPCG specimens under two 200 kg repeated explosions were 4.67% and 17.37%, respectively. Comparing the PG and PPCG specimens under two 200 kg repeated explosions, the displacement decreased by 11.73%.

The results show that after the first explosion, the top plate located directly beneath the blast center formed a rupture, allowing the shockwave from the second blast to enter the box girder, intensifying the impact on the baseplate. After applying the polyurea coating, the energy-absorption mechanism of polyurea dissipated much of the direct impact on the baseplate by converting internal energy into the fracture energy of the top plate's concrete. Consequently, the baseplate's displacement was reduced. Furthermore, polyurea's protective impact improved with higher explosive charges under repeated explosions.

(2) Multiple points and multiple detonations

From the aforementioned studies, it has been observed that when explosive loads act on the surface of an ultra-wide box girder, the typical failure mode involves localized punching shear failure. In military strikes, missiles and armor-piercing projectiles can cause explosions inside the box. These warheads, composed of high-strength material cores, penetrate the top plate due to the high velocity provided by the detonation of the propellant.

The projectile cores use their kinetic energy and material strength to pierce the top plate, allowing them to enter the chamber and explode, causing more extensive damage to the box girder. Additionally, in terrorist attacks, successive explosions may take place both externally and internally within the box. To further investigate the damage characteristics and dynamic response of ultra-wide box girders during internal explosions, the restart function of LS-DYNA was employed. The first explosion was set at the upper surface center, creating a localized penetration hole in the top plate. Afterward, a second explosion was placed inside the chamber. The design of multiple blast scenarios is presented in Table 10.

Table 10. Design of multiple blast scenarios.

Specimen	Condition	Number of Explosions	Blast Charge Position		Blast Height/m	TNT Charge/kg	Scaled Distance/(m/kg$^{1/3}$)
			Transverse Direction	Longitudinal Direction			
PG/PPCG	17	First	Top plate center of box chamber 1	Mid-span	1	200	0.171
		Second	Center of the interior of box chamber 1		1.077	200	0.184
	18	First	Top plate center in box chamber 2	Mid-span	1	200	0.171
		Second	Center of the interior of box chamber 2		1.041	200	0.178
	19	First	Top plate center in box chamber 3	Mid-span	1	200	0.171
		Second	Center of the interior of box chamber 3		1.017	200	0.174

Damage patterns of ultra-wide box girders under continuous repeated blasts, both inside and outside the box, are depicted in Figure 38. When the blast occurred above the top plate center of each compartment, both specimens PG and PPCG experienced local perforation damage to the top plate, while the web and baseplates showed no significant damage, with the steel bars at the rupture area bent and yielded. The second explosion occurred inside the box compartment, where the shock wave impacted the top, bottom, web plates, and diaphragm beam. In specimen PG, both the top plate and baseplate had perforations, and concrete spalling occurred on the rear-blast surfaces of both side webs and diaphragm beams. In specimen PPCG, only the top plate was perforated, with the baseplate remaining intact, and no significant spalling was observed on the side webs or the rear surface of the diaphragm beam. Compared to an explosion above the box girder, the internal explosion resulted in more extensive damage. The reason for this is that during the blast above the box girder, the top plate directly absorbs the blast wave, leading to localized damage, whereas during the internal explosion, the shock wave is confined by the walls, leading to multiple reflections and superimpositions, resulting in multiple impacts on the box, thus amplifying the damaging effect. The results show that polyurea coating significantly improved the blast resistance of the box girder, with the most noticeable improvement in chamber 3 at the boundary, where only minor concrete spalling occurred on the end face.

(3) Simultaneous detonation at multiple points

As analyzed in Section 4.2.2, the central section of the T-beam, the quarter-span points, and the outermost web are considered vulnerable areas. To investigate the impact of simultaneous detonation at various points on the blast resistance of the ultra-wide box girder coated with polyurea, explosive loads were applied at these three weak positions simultaneously, with a TNT charge of 500 kg and a detonation height of 1 m. The finite-element model for simultaneous detonation at multiple points of the ultra-wide box girder is shown in Figure 39.

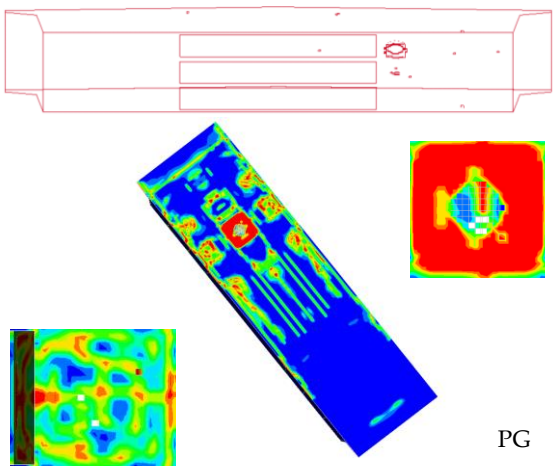

External explosion of 200 kg

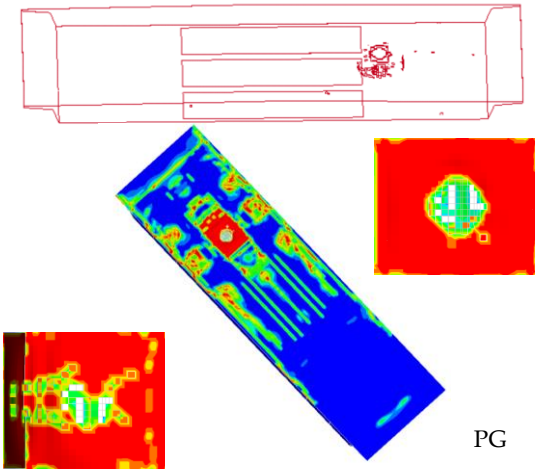

Internal explosion of 200 kg

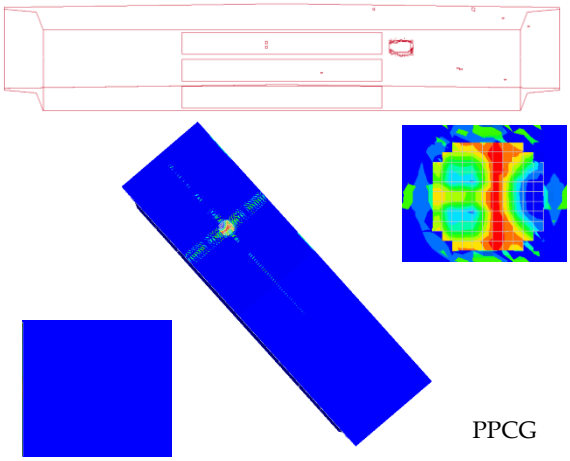

External explosion of 200 kg

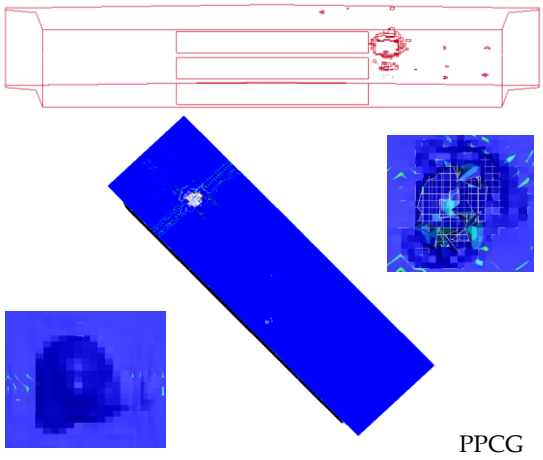

Internal explosion of 200 kg

(**a**) Condition 18 (box chamber 1)

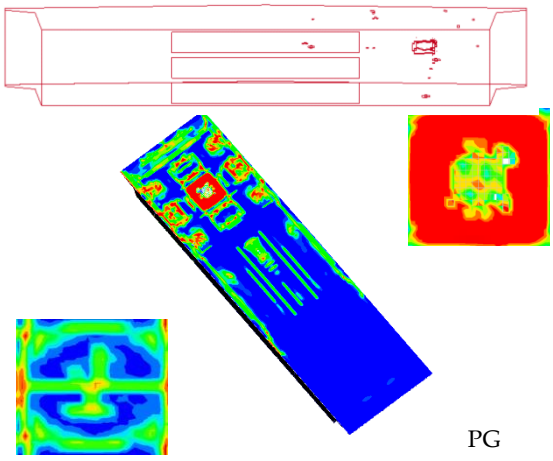

External explosion of 200 kg

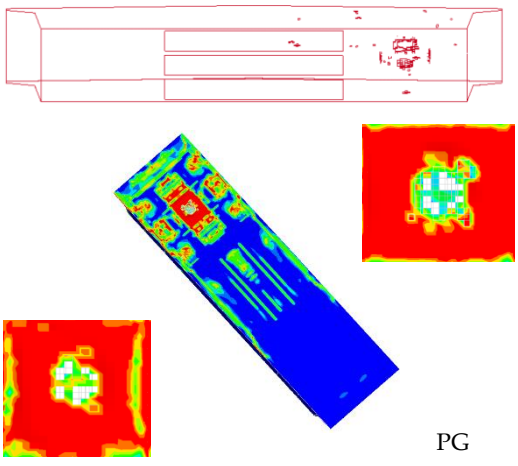

Internal explosion of 200 kg

Figure 38. *Cont*.

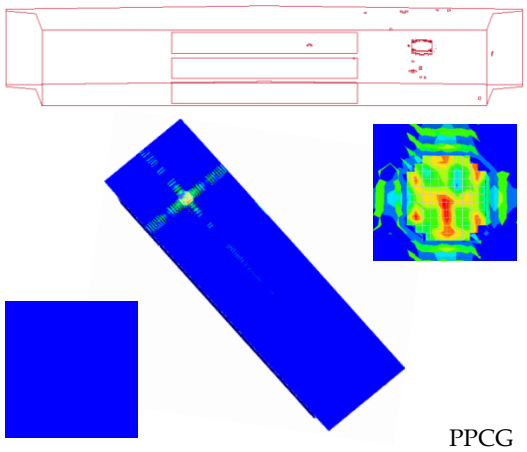

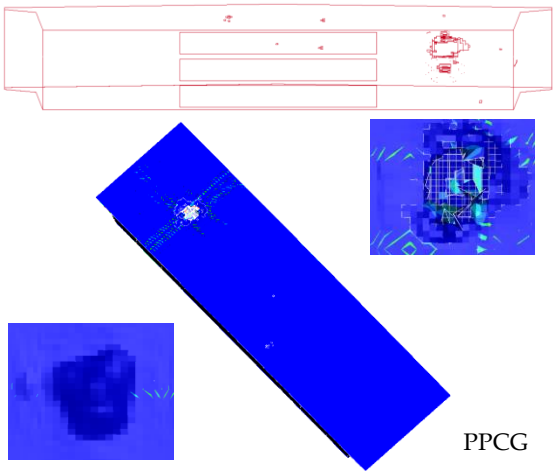

External explosion of 200 kg Internal explosion of 200 kg

(**b**) Condition 18 (box chamber 2)

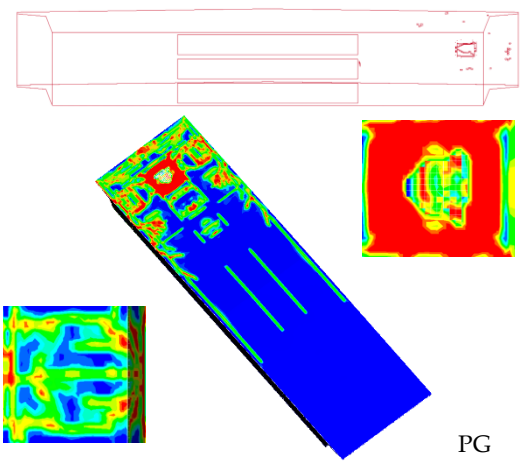

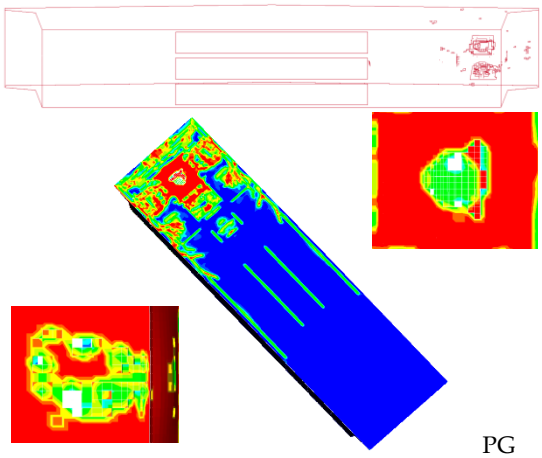

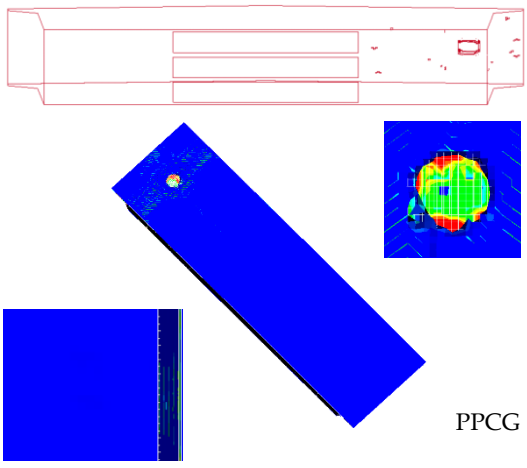

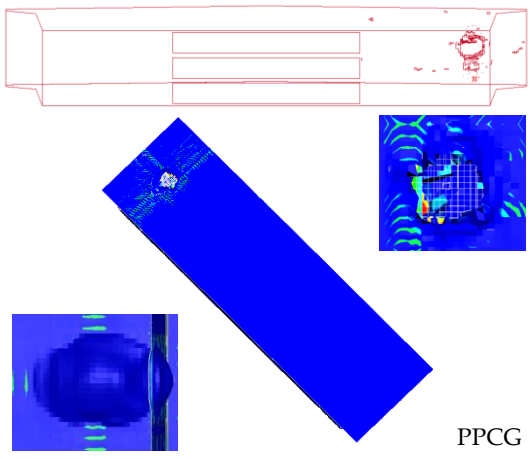

External explosion of 200 kg Internal explosion of 200 kg

(**c**) Condition 19 (box chamber 3)

Figure 38. Comparison of the damage morphology of ultra-wide box girders coated with polyurea before and after repeated external and internal explosions.

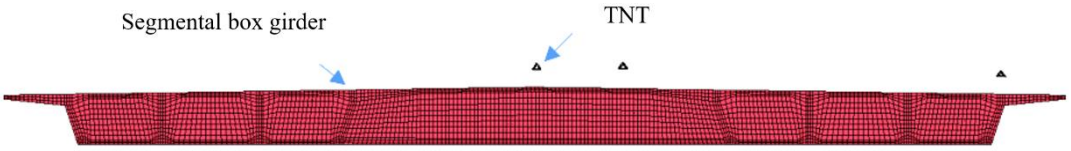

Figure 39. Finite-element model of ultra-wide box girder subjected to simultaneous multi-point explosions.

Figure 40 illustrates the damage characteristics of the polyurea-coated box girder under simultaneous detonation at multiple points. It can be observed from the figure that local perforations appeared on the top plate below the explosion centers in specimen PG, and the plastic strain was greatest near the perforations. The local strain gradually diffused outward and diminished. Due to the short distance from the T-beam center and the quarter-span points, a high-strain region connected the undamaged areas between the two perforations during simultaneous detonation. In specimen PPCG, the top plate under each explosion center was not fully perforated, and concrete spalling occurred on the top surface. Minor polyurea delamination and slight perforations were observed at the central and quarter-span points. The results indicate that simultaneous detonation at multiple points caused damage along the transverse axis of the bridge, reducing its overall strength and stability and significantly affecting its traffic capacity. However, after coating with polyurea, the overall blast resistance of the box girder was greatly enhanced, and it retained a certain level of traffic capacity.

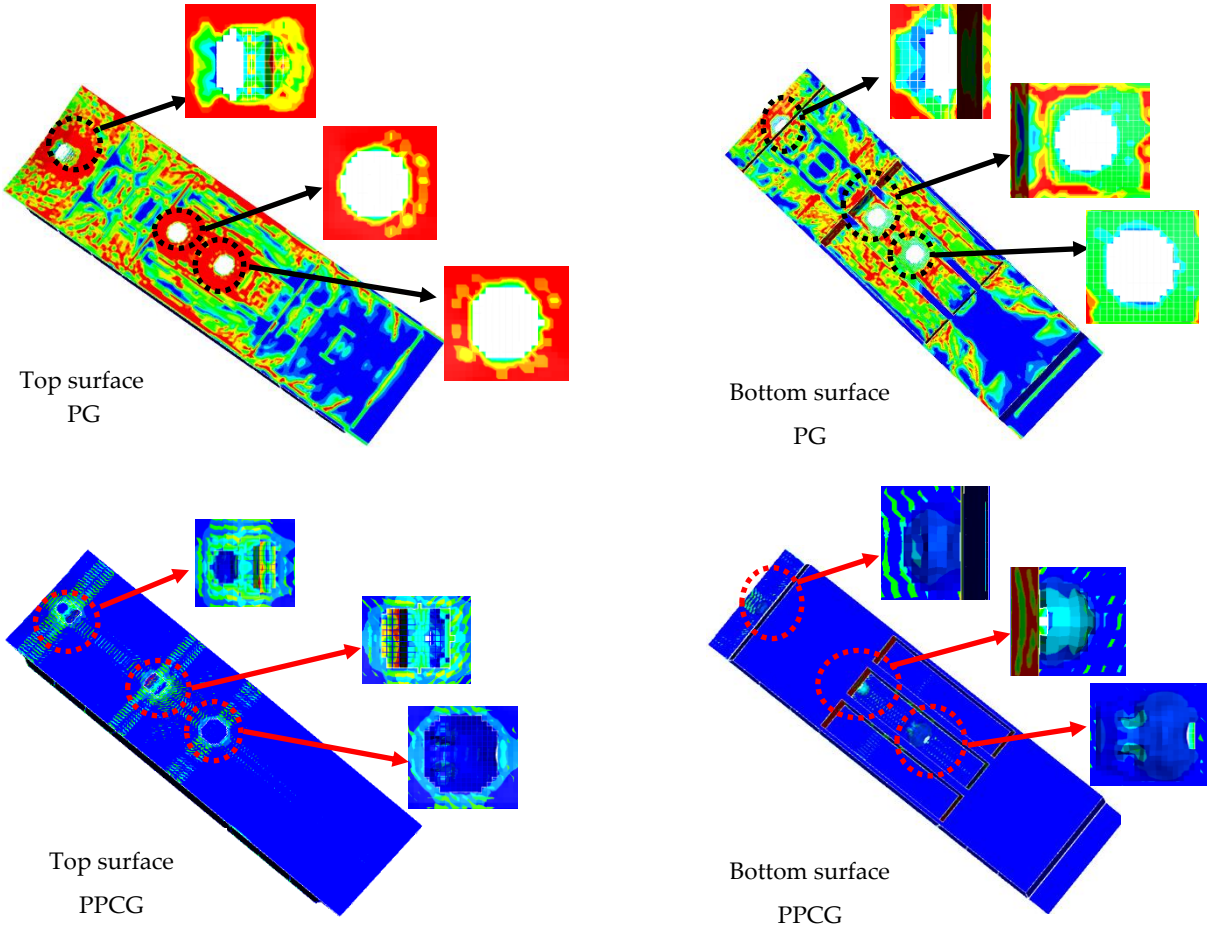

Figure 40. Damage pattern of ultra-wide box girder coated with polyurea under the charge of 500 kg with simultaneous multi-point explosions.

In summary, a comparative analysis was conducted on polyurea-coated box girders under three blast scenarios: single-point repeated detonation, multiple-point detonations, and simultaneous detonations. In terms of the extent of damage to the box girder, repair time, and traffic capacity, it was concluded that multiple-point repeated detonation (i.e., sequential detonation from the bridge surface to the interior of the box) caused the most severe damage. Nonetheless, after polyurea coating, the overall blast resistance improved significantly, with perforations occurring only in the top plate and no significant damage elsewhere, resulting in a relatively shorter repair time. Simultaneous detonation at multiple points caused several damage locations along the transverse axis, reducing the bridge's overall strength and stability while severely affecting traffic, but the polyurea coating substantially improved the blast resistance of the box girder, which still retained some traffic capacity.

4.2.4. Analysis of the Impact of Different Polyurea Thicknesses

The analysis in Section 4.2.2 shows that the central T-beam, quarter-span, and outer web are vulnerable points. To study the effect of the thickness of polyurea on blast resistance at these weak locations, simulations were performed with thicknesses ranging from 1.5 mm to 12 mm. The blast center was located 1 m above the mid-span, with a TNT equivalent of 500 kg. The different finite-element simulation cases for the weak regions with varying polyurea thicknesses are shown in Table 11. The vertical displacements of the baseplate at various points were recorded, starting from the initial point directly beneath the blast center and extending transversely across the bridge. The temporal evolution curves of the vertical shift and the peak shift at various points are depicted in Figure 41.

Table 11. Different polyurea thickness conditions.

Specimen	Condition	Polyurea Thickness/mm	Blast Charge Position		Blast Height/m	TNT Equivalent/kg	Scaled Distance/m/kg$^{1/3}$
			Transverse Direction	Longitudinal Direction			
PPCG	20	3	T-beam section center	Mid-span	1	500	0.171
	21	6					
	22	9					
	23	12					

As shown in Figure 41, the polyurea thickness significantly affects the vertical displacement of the baseplate beneath the blast center. When the polyurea coating thicknesses were 0 mm, 1.5 mm, 3 mm, 6 mm, 9 mm, and 12 mm, the corresponding vertical shift of the baseplate was 119.36 mm, 114.1 mm, 113.15 mm, 111.92 mm, 110.27 mm, and 110.23 mm, respectively. This indicates that increasing polyurea thickness reduces vertical displacement, enhancing blast resistance. At the center of the baseplate in the first box chamber, the vertical displacements for different polyurea thicknesses were 8.273 mm, 7.962 mm, 7.918 mm, 7.803 mm, 7.793 mm, and 7.603 mm, respectively. This trend further validates the positive correlation between polyurea thickness and the structure's blast resistance. At the baseplate center of box chamber 2, the vertical displacements for different polyurea thicknesses were 5.389 mm, 5.166 mm, 5.139 mm, 5.133 mm, 5.131 mm, and 5.129 mm, respectively. These findings confirm that increasing polyurea thickness reduces vertical displacement and boosts blast resistance. However, in the third box chamber, the vertical displacements for different polyurea thicknesses were 3.383 mm, 3.333 mm, 3.305 mm, 3.260 mm, 3.258 mm, and 3.241 mm, respectively. Although these data also show a correlation between polyurea thickness and vertical displacement, the trend is less pronounced in box chamber 3 than in the first two regions. In conclusion, increasing polyurea thickness enhances blast resistance, particularly in areas near the blast center. An optimal thickness of 9 mm is recommended.

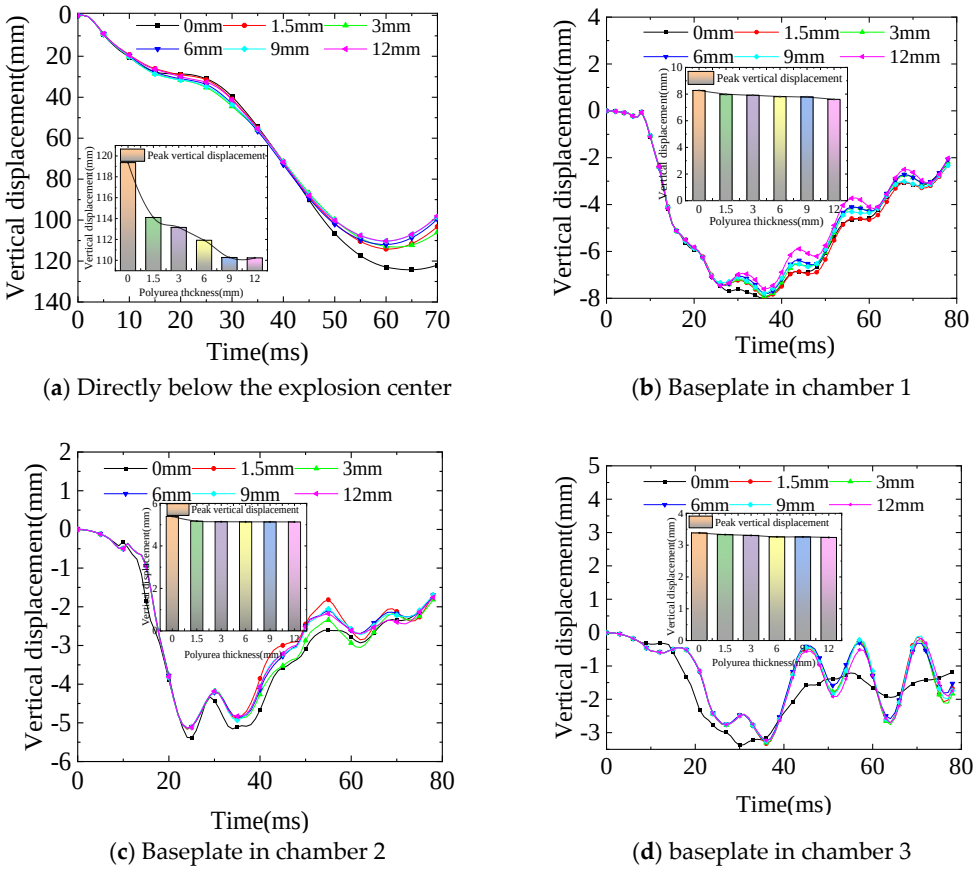

(**a**) Directly below the explosion center (**b**) Baseplate in chamber 1

(**c**) Baseplate in chamber 2 (**d**) baseplate in chamber 3

Figure 41. Vertical displacement of the baseplates of different box chambers under various polyurea coating thicknesses.

5. Conclusions

Test results showed that when two 3 kg TNT single explosions occurred, an elliptical hole appeared on the top plate of G, with slight bending of steel bars and extensive concrete spalling below. However, in PCG, the top plate coated with polyurea only showed slight indentation, indicating that the polyurea coating provided effective protection. During the secondary detonation of 5 kg of TNT, an elliptical hole was formed in the PCGR of the specimen, and some steel bars fractured and peeled off. Compared with specimen G, the peak and residual displacement increased by 606.2% and 619.5%, respectively, and the peak acceleration increased by 366.3%, indicating that the overall displacement under repeated explosive loads was much higher.

Numerical simulations showed that when a single explosion occurred above the ultra-wide concrete double-sided box beam, the top plate of the beam was subjected to the explosion load, and the stress and strain in the concrete rapidly increased, resulting in local penetration of the top plate. The bottom surface did not penetrate after coating with polyurea. The TNT equivalent was maintained at 200 kg, and only the lateral bridge explosion position was changed. The displacement reduction effect of polyurea coating on the near boundary area was particularly significant.

Multiple consecutive detonations (i.e., surface explosions, followed by internal box explosions) caused the most extensive damage to the box girder, but after the application of polyurea, the overall blast resistance was significantly improved. Only the surface peeling of the top concrete of the roof occurred, and no obvious damage was observed in other areas, resulting in a relatively short repair time. The simultaneous occurrence of multiple explosions along the transverse axis of the bridge caused multiple damage points, reducing the overall strength and stability of the structure and seriously affecting traffic.

However, after the application of polyurea, the overall blast resistance of the box girder was significantly improved, maintaining a certain level of traffic capacity.

The polyurea coating significantly reduces the vertical displacement of ultra-wide box girders, and this reduction slightly decreases with the increase of polyurea thickness, ultimately reaching a steady state. Therefore, for the ultra-wide concrete double-sided box girder in this study, it is recommended to use a 9 mm-thick polyurea coating to optimize its blast resistance under a 500 kg TNT explosion.

In this study, the polyurea was only applied to the transverse direction of the main girder of the self-anchored suspension bridge, excluding the longitudinal direction of the entire bridge as well as the main cables, hangers, main towers, and the interiors of each box segment. In future studies, it will be necessary to analyze the impact of polyurea in these areas. Additionally, this study simulated the explosive load using only the LBE method. In subsequent research, the ALE method should be employed to establish air and explosive models for a comparative analysis of the bridge's explosion response. Furthermore, the effects of different explosive shapes need to be considered and compared. However, it is essential to determine a reasonable air domain range and mesh size to avoid excessively long computation times.

Author Contributions: Software, R.W.; Formal analysis, R.W.; Investigation, R.W.; Data curation, R.W.; Writing—original draft, R.W., Project administration, G.Z.; Funding acquisition, G.Z., Writing—review & editing, G.Z.; Validation, G.Z., Methodology, X.Z.; Supervision, X.Z. All authors have read and agreed to the published version of the manuscript.

Funding: This research was funded by G.Z grant number BK20200494, 2021M701725, 2021K522C. And The APC was funded by BK20200494.

Data Availability Statement: The original contributions presented in the study are included in the article, further inquiries can be directed to the corresponding author.

Conflicts of Interest: The authors declare no conflict of interest.

References

1. Nettis, A.; Nettis, A.; Ruggieri, S.; Uva, G. Corrosion-induced fragility of existing prestressed concrete girder bridges under traffic loads. *Eng. Struct.* **2024**, *314*, 118302. [CrossRef]
2. Nettis, A.; Nettis, A.; Ruggieri, S.; Uva, G. Typological fragility assessment of prestressed concrete girder bridges subjected to traffic loads affected by corrosion. In Proceedings of the COMPDYN 2023 9th ECCOMAS Thematic Conference on Computational Methods in Structural Dynamics and Earthquake Engineering, Athens, Greece, 12–14 June 2023; pp. 5242–5257.
3. Luca, T.; Enrica, V.; Stefano, G. Performance of Atlas GNSS Global Correction Service for High-Accuracy Positioning. *J. Surv. Eng.* **2021**, *147*, 05021005.
4. Marco, Z.; Emanuele, R.; Nicola, L.; Victor, E.; Pietro, C. On the structural behavior of existing RC bridges subjected to corrosion effects: Numerical insight. *J. Surv. Eng.* **2023**, *152*, 107500.
5. Stergiou, T.; Baxevanakis, K.P.; Roy, A.; Sazhenkov, N.A.; Nikhamkin, M.S.; Silberschmidt, V.V. Impact of polyurea-coated metallic targets: Computational framework. *Compos. Struct.* **2021**, *267*, 113893. [CrossRef]
6. Grujicic, M.; D'entremont, B.P.; Pandurangan, B.; Runt, J.; Tarter, J.; Dillon, G. Concept-level analysis and design of polyurea for enhanced blast-mitigation performance. *J. Mater. Eng. Perform.* **2012**, *21*, 2024–2037. [CrossRef]
7. Ackland, K.; Anderson, C.; Ngo, T. Deformation of polyurea-coated steel plates under localized blast loading. *Int. J. Impact Eng.* **2013**, *51*, 13–22. [CrossRef]
8. Amini, M.; Isaacs, J.; Nemat-Nasser, S. Investigation of effect of polyurea on response of steel plates to impulsive loads in direct pressure-pulse experiments. *Mech. Mater.* **2010**, *42*, 628–639. [CrossRef]
9. Amini, M.; Amirkhizi, A.; Nemat-Nasser, S. Numerical modeling of response monolithic and bilayer plates to impulsive loads. *Int. J. Impact Eng.* **2010**, *37*, 90–102. [CrossRef]
10. Zeng, L.; Liang, H.; Liu, L.; Zhang, Q. Anti-explosion design method for aluminum alloy doors in ordinary buildings. *J. Fail. Anal. Prev.* **2021**, *21*, 268–279. [CrossRef]
11. Gu, M.; Ling, X.; Yu, A.F.; Chen, G.X.; Wang, H.Z.; Wang, H.X. Experimental study of polyurea-coated fiber-reinforced cement boards under gas explosions. *Def. Technol.* **2023**, *23*, 201–213. [CrossRef]
12. Davidson, J.S.; Porter, J.R.; Dinan, R.J.; Hammons, M.I.; Connell, J. Explosive testing of polymer retrofit masonry walls. *J. Perform. Constr. Facil.* **2004**, *18*, 100–106. [CrossRef]
13. Pu, X.F. *Numerical Analysis of Explosion Response of Elastomer Reinforced Concrete Masonry Wall*; Ningbo University: Ningbo, China, 2019. (In Chinese)

14. Baylot, J.T.; Bullock, B.; Slawson, T.R.; Woodson, S.C. Blast Response of Lightly Attached Concrete Masonry Unit Walls. *J. Struct. Eng.* **2005**, *131*, 186–193. [CrossRef]
15. Samiee, A.; Amirkhizi, A.V.; Nemat-Nasser, S. Numerical study of the effect of polyurea on the performance of steel plates under blast loads. *Mech. Mater.* **2013**, *64*, 1–10. [CrossRef]
16. Wang, Y. *Research on Response of Self-Anchored Suspension Bridge under Static and Dynamic and Explosive Shock Waves*; Chan'an University: Xi'an, China, 2020. (In Chinese)
17. Yang, Z. *Dynamic Response Study of Reinforced Concrete Box Girder under Blasting Load*; National University of Defense Technology: Changsha, China, 2019. (In Chinese)
18. Qiu, M.J. *Research on Dynamic Response and Failure Mechanism of Prestressed Concrete Bridge Structure under Blast Load*; Xi'an University of Technology: Xi'an, China, 2021. (In Chinese)
19. Fujikura, S.; Bruneau, M. Experimental investigation of seismically resistant bridge piers under blast loading. *J. Bridge Eng.* **2011**, *16*, 63–71. [CrossRef]
20. Williams, G.D.; Williamson, E.B. Response of reinforced concrete bridge columns subjected to blast loads. *J. Struct. Eng.* **2011**, *137*, 903–913. [CrossRef]
21. Echevarria, A.; Arash, B.; Zaghi, A.E.; Chiarito, V.; Christenson, R.; Woodson, S. Experimental comparison of the performance and residual capacity of CFFT and RC bridge columns subjected to blasts. *J. Bridge Eng.* **2016**, *21*, 04015026. [CrossRef]
22. Williamson, E.B.; Bayrak, O.; Avis, C. Performance of bridge columns subjected to blast loads. *J. Bridge Eng.* **2011**, *16*, 693–702. [CrossRef]
23. Islam, A.; Yazan, N. Performance of AASHTO girder bridges under blast loading. *Eng. Struct.* **2007**, *30*, 1922–1937. [CrossRef]
24. Maazoun, A.; Vantomme, J.; Matthys, S. Damage assessment of hollow core reinforced and prestressed concrete plates subjected to blast loading. *Procedia Eng.* **2017**, *199*, 2476–2481. [CrossRef]
25. Han, G.Z.; Yan, B.; Yang, Z. Damage model test of prestressed T-beam under explosion load. *IEEE Access* **2019**, *7*, 135340–135351.
26. Yao, S.J.; Jiang, Z.G.; Lu, F.Y.; Zhang, D.; Zhao, N. Analysis on local damage of steel box girder under internal blast loading of vehicle bomb. *J. Vib. Shock* **2015**, *34*, 222–227. (In Chinese)
27. Hashemi, S.; Bradford, M.; Valipour, H. Dinamic response of cable-stayed bridge under blast load. *Eng. Struct.* **2016**, *127*, 719–736. [CrossRef]
28. Hajek, R.; Flar, J.; Pachman, J. An experimental evaluation of the blast resistance of heterogeneous concrete-based composite bridge decks. *Eng. Struct.* **2019**, *179*, 204–210. [CrossRef]
29. Zhou, G.P.; Lin, Z.C.; Wang, M.Y.; Fan, J.; Wang, R.; He, Z. Effect change of extra-wide concrete self-anchored suspension bridge under blast loads and its prediction considering time-dependent effect. *Structures* **2023**, *50*, 1035–1050. [CrossRef]
30. Zhou, G.; Wang, R.; Wang, M.; Ding, J.; Zhang, Y. Explosion resistance performance of reinforced concrete box girder coated with polyurea: Model test and numerical simulation. *Def. Technol.* **2023**, *33*, 1–18. [CrossRef]
31. Liu, Q.; Chen, P.W.; Guo, Y.S.; Su, J.J.; Han, L.; Arab, A.; Yuan, J.F. Mechanical behavior and failure mechanism of polyurea nanocomposites under quasi-static and dynamic compressive loading. *Def. Technol.* **2020**, *17*, 495–504. [CrossRef]
32. Liu, Q.; Guo, B.; Chen, P.; Su, J.; Arab, A.; Ding, G.; Guo, F. Investigating ballistic resistance of CFRP/polyurea composite plates subjected to ballistic impact. *Thin-Walled Struct.* **2021**, *166*, 108111. [CrossRef]
33. Malvar, L.J.; Crawford, J.E.; Wesevich, J.W.; Simons, D. A plasticity concrete material model for YNA3. *Int. J. Impact Eng.* **1997**, *19*, 847–873. [CrossRef]
34. Holmquist, T.J.; Johnson, G.R.; Cook, W.H. A computational constitutive model for concrete subjected to large strains, high strain rates, and high pressure. In Proceedings of the 14th International Symposium on Ballistics, Quebec City, QC, Canada, 26–29 September 1993; pp. 591–600.
35. Zhang, S.Y.; Zong, Q.; Lyv, N. Numerical simulation of the anti-explosion protective damage effect of polyurea coating on caisson docks. *J. Saf. Sci. Technol.* **2021**, *17*, 162–168. (In Chinese)
36. Zhou, G.P. *Research on the State Control and Spatial Mechanical Behavior of Ultra-Wide Concrete Self-Anchored Suspension Bridge after Completion*; Southeast University: Nanjing, China, 2018.
37. Shiravand, M.; Parvanehro, P. Numerical study on damage mechanism of post-tensioned concrete box bridges under close-in deck explosion. *Eng. Fail. Anal.* **2017**, *81*, 103–116. [CrossRef]
38. Eibeck, A.; Shaocong, Z.; Mei Qi, L.; Kraft, M. Analysis of the Influence Law of Missile Strike Position on Box Beam Invasion and Explosion amage. *Def. Transp. Eng. Technol.* **2019**, *17*, 20–23. (In Chinese)
39. Federal Emergency Management Agency (FEMA). *Reference Manual to Mitigate Potential Terrorist Attacks against Buildings*; Government Printing Office: Washington, DC, USA, 2003; FEMA426; pp. 24–30.
40. Kong, X.L.; Jin, F.N.; Jiang, M.R. Analysis of terrorist bombing attack mode and scale. *Blast* **2007**, *3*, 88–92. (In Chinese)